

Comprehensive Summaries of Uppsala Dissertations
from the Faculty of Science and Technology 885



Segmentation and Visualisation of Human Brain Structures

BY

ROGER HULT



ACTA UNIVERSITATIS UPSALIENSIS
UPPSALA 2003

Dissertation at Uppsala University to be publicly examined in sal X, Universitetshuset, Friday, October 10, 2003 at 10:15 for the Degree of Doctor of Philosophy. The examination will be conducted in Swedish

Abstract

Hult, R. 2003. Segmentation and Visualisation of Human Brain Structures. Acta Universitatis Upsaliensis. *Comprehensive Summaries of Uppsala Dissertations from the Faculty of Science and Technology* 885. 68 pp. Uppsala. ISBN 91-554-5729-0

In this thesis the focus is mainly on the development of segmentation techniques for human brain structures and of the visualisation of such structures. The images of the brain are both anatomical images (magnet resonance imaging (MRI) and autoradiography) and functional images that show blood flow (functional magnetic imaging (fMRI), positron emission tomography (PET), and single photon emission tomography (SPECT)). When working with anatomical images, the structures segmented are visible as different parts of the brain, e.g. the brain cortex, the hippocampus, or the amygdala. In functional images, the activity or the blood flow that be seen.

Grey-level morphology methods are used in the segmentations to make tissue types in the images more homogenous and minimise difficulties with connections to outside tissue. A method for automatic histogram thresholding is also used. Furthermore, there are binary operations such as logic operation between masks and binary morphology operations.

The visualisation of the segmented structures uses either surface rendering or volume rendering. For the visualisation of thin structures, surface rendering is the better choice since otherwise some voxels might be missed. It is possible to display activation from a functional image on the surface of a segmented cortex.

A new method for autoradiographic images has been developed, which integrates registration, background compensation, and automatic thresholding to get faster and more reliable results than the standard techniques give.

Keywords: segmentation, visualisation, brain, cortex, hippocampus, autoradiography, MRI, PET, ROI

*Roger Hult, Centre for Image Analysis. Uppsala University.
Lägerhyddsvägen 3, SE-752 37 Uppsala, Sweden*

© Roger Hult 2003

ISBN 91-554-5729-0
ISSN 1104-232X

Printed in Sweden by University Printers, Uppsala University, Uppsala, 2003
urn:nbn:se:uu:diva-3567 (<http://urn.kb.se/resolve?urn=urn:nbn:se:uu:diva-3567>)

In memory of my mother
Kerstin Hult

Acknowledgments

The scientific work carried out during the project has been carried out at the Centre for Image Analysis, Uppsala University, Sweden and at Human Brain Informatics, Department of Clinical Neuroscience, Psychiatry Section Karolinska Institutet, Stockholm, Sweden. The financial support from the National Swedish Board of Technical Development under grant number 4067-7 is gratefully acknowledged. The work was carried out in close collaboration with the VISIT program of the Foundation for Strategic Research.

First of all, I would like to thank my supervisors. Professor Ewert Bengtsson has helped and guided me during my years here at CBA: I am especially grateful for his calling me from Siberia to provide me with help in the last week of writing this thesis. I would also like to thank Docent Lennart Thurfjell, who introduced me to the many aspects of image analysis in general and images of the brain in particular. I am grateful for his valuable comments on this thesis and for many other things. Docent Ingrid Agartz provided me with challenging problems to solve which resulted in a couple of publications. Docent Håkan Hall supported me in my doctoral studies at a crucial moment. He also provided me with scientific help in the area of biochemistry, which is not one of the subjects I have studied.

I would also like to thank all my colleagues, current and former, at the Centre for Image Analysis for providing a nice and creative atmosphere to work in. Many of you are also part of my life outside of CBA. Those not mentioned here are not forgotten! I am grateful to Professor Gunilla Borgefors for her support in scientific and other matters concerning my work here at CBA, and for valuable discussions. Dr. Roger Lundqvist has been a sounding board for ideas and provided help with understanding how to program the PC version of CBA. I am grateful to Felix Wehrmann for all our valuable scientific and non-scientific discussions and all the adventures that we have shared in different parts of the Nordic countries, and to Joakim Lindblad for helping me use his methods and assisting me in installing them on my PC. Without Docent In-

gela Nyström this dissertation would never have come into existence, since she introduced me to the field of image analysis in the first place, during the undergraduate course. I would also like to thank her for valuable input on scientific matters, such as suggestions on this thesis. Dr. Olle Eriksson has solved many computer-related problems, and exhibited an acerbic sense of humour while doing so. Bosse never became IMPatient with my questions concerning IMP. I would like to thank Mattias Aronson for always being eager to discuss scientific matters and sharing code with me. Lena Wadelius has always been helpful with matters concerning administration and she has answered all my questions on things not always directly linked to my research. I would like to thank Hans Frimmel for scientific discussions and many other things, Petter Ranefall who shared my room for some years and told me about the undergraduate work that resulted in my ending up as a doctoral student at CBA, and Mikael Vondrus for our discussions on different matters.

Thanks are also due to all my current and former colleagues at Karolinska Hospital. I am grateful to Marita Signarsson for making administrative matters easy, and to Katarina Varnäs for introducing me to new areas in brain research and for many valuable discussions.

Despite attempts in that direction, I have not been able to spend my entire waking time in writing this dissertation. I would like to thank all my friends in the Society for Creative Anachronism (SCA), for all the events, dancing, late night tea-times, chit-chat and discussions of more importance. Irene Karlsson Elfgren and Johan Elfgren were there for me when I really needed it. Cecilia Anéer has always shared the time that she really did not have. I am grateful to Veronika Hallberg for her friendship. I would like to thank Marit Carlsson who has contributed significantly by proof-reading my articles and my undergraduate thesis. I am grateful for the support she gave me in moments when I despaired during my doctoral studies.

I would like to thank Kristina Hildebrand who housed me and fed me and pushed me when it was necessary during the last two years of my doctoral studies. I am also grateful for the professional linguistic assistance she has provided in the last few weeks of writing this thesis.

I would like to thank Josefin Klasson for being a good friend ever since we met in the line outside the School of Engineering Studies Office.

I would like to thank Anders Ingvarsson, Henning Janson, and Peter Öhrt, who have been my very good friends all my life.

I would like to thank Adde Wikestedt for a long friendship, with countless interesting discussions and also for the activities in the studio we used to share. I look forward to making music with you again soon.


I would also like to thank Henrik Malm for being a good friend, Rickard Hidefjäll for encouraging me when I really needed it, and both of them for the times when we composed music together.

Much of this dissertation was written with a dog clinging to my arm. Isa never nagged me about anything except her food, her walks, or her playtime, and only rarely tried to walk on my hands.

I would like to thank all my relatives for being there for me. In particular, I would like to thank my mother Kerstin for all her support when I needed it. I really wish she could be here with me now. My father Lennart and my grandparents have always been supporting me.

Finally, I would like to thank all people who have been a part of my life at different times. You are not at all forgotten.

Uppsala 31 August, 2003

A handwritten signature in black ink, appearing to read 'Roger Hult', with a stylized, flowing script.

Roger Hult

Included papers

This thesis is based on the following papers, referred to in the text by their Roman numerals:

- I **“Surface Construction Especially Suited for Visualisation of Thin Structures”**
R. Hult, E. Bengtsson, L. Thurfjell, Proceedings of 10th *Scandinavian Conference on Image Analysis, SCIA’97*: , Lappeenranta, Finland, 2149–2154 (1997).
- II **“Automatic Detection of Hypoperfused Areas in SPECT Brain Scans”**
L. Thurfjell, J. Andersson, M. Pagnani, C. Jonsson, R. Hult, R. Lundqvist, A. Wagner, H. Jacobsson, S. Larsson, *IEEE Transactions on Nuclear Science*, vol 45, no 4, 2149–2154, (1998), © by IEEE.
- III **“Segmentation of the Brain in MRI Using Grey Level Morphology and Propagation of Information”**
R. Hult, E. Bengtsson, L. Thurfjell, Proceedings of 11th *Scandinavian Conference on Image Analysis, SCIA’99*, Kangerlussuaq, Greenland, 367–373 (1999).
- IV **“Combined Visualisation of Functional and Anatomical Brain Images”**
R. Hult, E. Bengtsson, Proceedings of 12th *Scandinavian Conference on Image Analysis, SCIA 2001*, Bergen, Norway, 84–89 (2001) .
- V **“Grey-level Morphology Based Segmentation of MRI of the Human Cortex”**
R. Hult, Proceedings of *ICIAP’01 11th International Conference on Image Analysis and Processing*, Palermo, Italy, 578–583, (2001), © by IEEE.
- VI **“Segmentation of T1-MRI of the Human Cortex Using a 3D Grey-level Morphology Approach”**
R. Hult, *Image Analysis*, 13th *Scandinavian Conference on Image Analysis, SCIA2003*, Halmstad, Sweden, June/July 2003, Proceedings, 462–469, (2003), © by Springer.
- VII **“Grey-level Morphology Combined with an Artificial Networks Approach for Multimodal Segmentation of the Hippocampus”**
R. Hult, Proceedings of *ICIAP’03 12th International Conference on Image Analysis and Processing*, Mantua, Italy, (2003), © by IEEE.
- VIII **“Image Analysis of Co-registered Autoradiographic Human Whole Hemisphere Sections”**
R. Hult, K. Varnäs, H. Hall. Manuscript.
- IX **“Segmentation of Multimodal MRI of Hippocampus Using 3D Grey-level Morphology Combined with Artificial Neural Networks”**
R. Hult, I Agartz, Manuscript.

All papers published, in press or accepted for publication are reproduced with permission from the publisher. The papers in this thesis have been checked for

errors and thus differ somewhat from the published version.

Faculty opponent is Dr. Arvid Lundervold, University of Bergen, Bergen, Norway.

In the process of performing the research leading to this thesis, the author has contributed also to the following publications:

- i **“3D Reconstruction of Insects’ Ganglion”**
R. Hult, Proceedings of SSAB (*Swedish Society for Automated Image Analysis*) Symposium on Image Analysis, Lund, Sweden, 91–95 (1996).
- ii **“Grey-level Morphology Based Segmentation of Cortex”**
R. Hult, Proceedings of SSAB (*Swedish Society for Automated Image Analysis*) Symposium on Image Analysis, Norrköping, Sweden, 151–154, (2001).
- iii **“Grey-level Morphology Based Segmentation of T1-MRI of the Human Cortex”**
R. Hult, Proceedings of *Medical Image Computing and Computer-Assisted Intervention – MICCAI 2001 4th International Conference*, Utrecht, The Netherlands, 1371–1372, (2001).

The author has participated in the following external conferences and courses:

- SSAB'96 (Swedish Society for Automated Image Analysis, annual symposium), Lund, March 7–8, 1996. Paper i - Oral presentation.
- CNSoftware Limited Analyze 7C Training Course, Crawley, England, May 23–24, 1996.
- VBC'96 (Visualization in Biomedical Computing), Hamburg, Germany, September 22–25, 1996.
- SCIA'97 (10th Scandinavian Conference on Image Analysis), Lappeenranta, Finland, June 9–11, 1997. Paper I - Poster presentation.
- SSAB'97 (Swedish Society for Automated Image Analysis, annual symposium), Stockholm, March 4–5, 1997.
- SSAB'98 (Swedish Society for Automated Image Analysis, annual symposium), Uppsala, March 16–17, 1998.
- Summer School in Shape Variation '98, Copenhagen, Denmark, August, 1998.
- SSAB'99 (Swedish Society for Automated Image Analysis, annual symposium), Göteborg, March 9–10, 1999.
- SCIA'99 (11th Scandinavian Conference on Image Analysis), Kangerlussuaq, Greenland, June 9–11, 1999. Paper III - Oral presentation.
- DGCI 2000 (9th International Conference on Discrete Geometry for Computer Imagery), Uppsala, Sweden, December 13–15, 2000.
- SSAB'01 (Swedish Society for Automated Image Analysis, annual symposium), Norrköping, Sweden, March 14–15, 2001. Paper ii - Oral presentation.
- SCIA'01 (12th Scandinavian Conference on Image Analysis), Bergen, Norway, June 11–14, 2001. Paper IV - Poster presentation.
- Third Annual Brain Imaging Workshop, Iowa City, USA, August 7–10, 2001.
- ICIAP'01 (11th International Conference on Image Analysis and Processing), Palermo, Italy, September 26–28, 2001. Paper V - Oral presentation.
- MICCAI'01 (4th International Conference of Medical Image Computing and Computer-Assisted Intervention), Utrecht, The Netherlands, October 14–17, 2001. Paper iii - Poster presentation.
- SSAB'03 (Swedish Society for Automated Image Analysis, annual symposium), KTH, Stockholm, March 6–7, 2003.
- SCIA'03 (13th Scandinavian Conference on Image Analysis), Gothenburg, Sweden, June 29 – July 2, 2003. Paper VI - Oral presentation.
- ICIAP'03 (12th International Conference on Image Analysis and Processing), Mantua, Italy, September 17–19, 2003. Paper VII - Poster presentation.

Contents

Acknowledgments	v
1 Introduction	1
1.1 Modalities	4
1.1.1 Magnetic Resonance Imaging (MRI)	5
1.1.2 Computed Tomography (CT)	6
1.1.3 Positron Emission Tomography (PET)	6
1.1.4 Single Photon Emission Computed Tomography (SPECT)	7
1.2 Registration	7
1.3 The IMage Processing (IMP) Environment	8
1.4 The Computerised Brain Atlas (CBA) Project	8
1.5 The BRAINS2 Software	10
2 Methods Used in Brain Segmentation	13
2.1 Grey-level Morphology	13
2.2 Segmentation of the Cortex from MRI	17
2.2.1 A Short Survey of Segmentation Techniques Used to Segment the Cortex	17
2.2.2 An Overview of the Progress of our Grey-level Morphology-Based Segmentation	18
2.2.3 An Overview of our Grey-level Morphology-Based Segmentation	20
2.3 Segmentation of the Hippocampus from Multivariate MRI	24
3 Visualisation Techniques	31
3.1 Visualisation of Thin Structures	32
3.2 Visualisation of Functional Information	33
3.2.1 Normal material for viewing Functional Information	33
3.2.2 3D Visualisation of Functional Information	34
4 Autoradiography	39
5 Conclusion	45
5.1 Discussion	45
5.2 Future Work and Improvements	47
References	49
Explanations of symbols, acronyms, abbreviations, and terms	61
Colour Plates	65

CHAPTER 1

Introduction

When working with medical images it is often of interest to delineate interesting areas or volumes. The process of finding those is called segmentation. One of the main contributions of the research described in this thesis is a method for automatic brain segmentation from T1-weighted MRI. Finding the cortex is important for several reasons. It is of interest to calculate the volume of the brain when performing research on it, as this can be used to compensate for differences in brain size. The segmented cortex can also be used to visualise the brain surface or for viewing activity beneath the surface on activation studies. For other structures, it is also desirable to measure the volume or, in some cases, the area in one slice. When studying, e.g. different psychiatric diseases it may be of interest to investigate whether or not a particular structure is smaller or larger on patients compared to normal material.

The rapid development of different kinds of 3D medical scanners and the increased use of such images have made it hard for the physicians to interpret and make diagnosis. There is a great need for automatic methods that process, and help with the interpretation of, the huge amounts of data that are available to physicians.

It only takes a few minutes to obtain a volume from a scanner, but manual interpretation may take hours and does not always lead to the same result on the same data set, especially if the volume-images are converted to a set of transparent prints. The reproducibility is important to keep subjectivity to a minimum. The robustness of algorithms used for diagnostics is very important. This is true even if the algorithm is used only to aid the interpretation of the images, and not for making decisions.

This thesis deals mostly with the segmentation of structures in the human brain from magnetic resonance images (MRI). Segmentation subdivides an image into objects of interest. These objects are often referred to as regions of interest (ROI) or volumes of interest (VOI); herein all objects are called ROIs whether they are 2D or 3D. This object is stored in a mask in which every position corresponds to the same position in the image segmented. In

images of the brain it is often important to segment the cortex from non-cortex tissues such as eyes and membranes of the brain. The skin, too, is in the way of viewing the brain. It is not trivial to segment the cortex of the brain as it is connected to extra brain tissue through, for example, nerves, and the connecting tissue often has the same grey level as the grey or white substance of the brain. This implies that it is not possible to use thresholding. If we try this strategy, there will always be some connections to non-brain tissue and the result would be an object that is much larger than desired. An approach often used is thresholding each slice manually and unwanted objects are erased manually.

Another part of the brain is studied within the scope of this thesis is the hippocampus. This is a bent structure with head, body, and tail. The hippocampus is hard to delineate using automatic methods, mainly because of its being a bent structure and changing extensively in all three slicing directions. It is also difficult to separate the hippocampus from the neighbouring brain structures.

In this thesis images of the brain, either 2D or 3D, are considered. The images used herein come from several different sources: magnetic resonance images (MRI), functional magnetic resonance imaging (fMRI), positron emission tomography (PET), single photon emission tomography (SPECT), autoradiography of cryosections. The first four modalities are tomographic 3D images and the last modality is 2D sections which may also be combined into a 3D volume.

A photo is a 2D image, extending in two directions. A digital image has been discretised both in spatial coordinates and in brightness. It can be considered a matrix, the row (y) and column (x) indices of which identify a point and the corresponding element identifies the grey level or colour. Figure 1.1a) shows the coordinate-system for a 2D image. The elements of a digital 2D image is called picture elements, or pixels for short. For volumes, the third dimension is orthogonal to the image plane in a 2D image. A volume can be seen as a stack of 2D images or slices. For each volume picture element, called voxel, a grey level is stored and can be accessed through the function $f(x, y, z)$. Figure 1.1b) shows the coordinate-system for a 3D image.

The 3D data used herein they should always be considered as 3D volumes and not as 2D slices. The algorithms described in this thesis are more 3D than 2D. There is no way of viewing 3D data without manipulation of some sort. If we are interested in seeing the surface of a head that has been acquired in an MR scanner, the background has to be removed, that is, thresholded. Still, the 2D screen cannot display the 3D data directly; first the data has to be projected in some way onto the 2D display. There are ways of seeing depth on a monitor, but this is also not real 3D since the display technique is sending two different 2D projections, one for each eye. This means that 3D volumes can only be

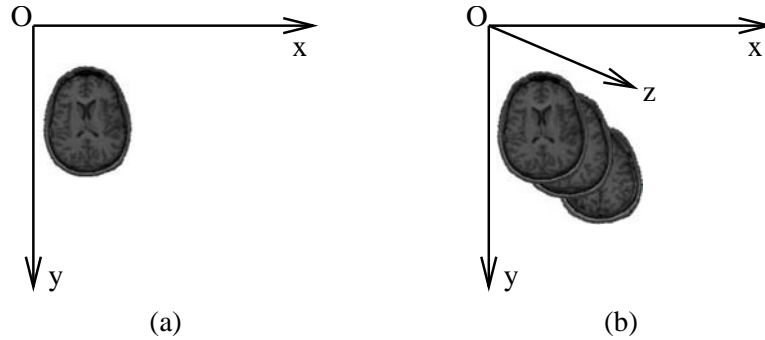


Figure 1.1: 2D and 3D coordinate systems. a) An image is spanned with two orthogonal axes. b) A volume is spanned with three orthogonal axes.

viewed by looking at a 2D projection of the volume. For an example of a 3D visualisation of brain data and the cortex, see Figure 1.2. In chapter 3, different techniques for visualising 3D volume data are described. Still, it is common that people who work with volume images look at slices only. There are several reasons for this, such as the person viewing the volume being accustomed to viewing slices, and it being hard for computers to produce 3D visualisation of good quality in real time.

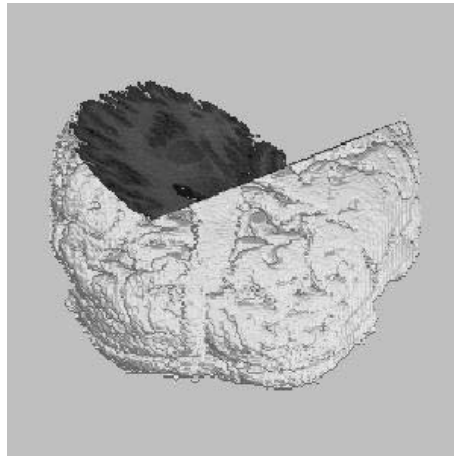


Figure 1.2: Visualisation of a segmented brain with the underlying structures shown by using two intersecting cut-planes.

If a volume is isotropic, the resolution in all three directions is the same. Most volumes acquired in medical scanners are anisotropic in at least one direction, this means that the voxels are not cubic and the dimensions must be saved with the data, otherwise all measurements in the volume would be impossible to interpret correctly. Transaxial images are acquired images in the x –

and y -plane as defined in Figure 1.1b). Depending on the protocol used, the resolution in the z direction can be changed. Higher resolution requires longer acquisition time. There are two more directions from which tomographic volumes of the brain are acquired: sagittal, i.e. viewed from the side of the head, and coronal, i.e. viewed from the back of the head. Figure 1.3 shows a transaxial, a sagittal and a coronal view of an MRI scan. They are usually isotropic in the acquisition plane with a lower resolution in the acquisition direction.

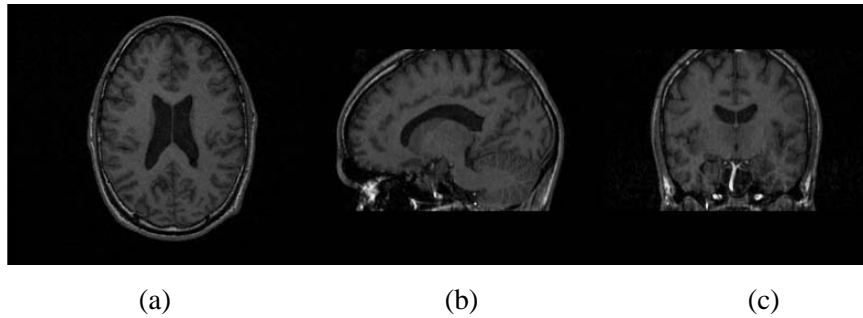


Figure 1.3: A brain viewed from three directions. a) A transaxial view. b) A sagittal view. c) A coronal view.

1.1 Modalities

In neuro-imaging there are two different kinds of modalities that provide complementary information: anatomical modalities and functional modalities. Within these two types there are several different modalities. Computed Tomography (CT) and standard magnetic resonance imaging (MRI) provide different aspects of anatomy, but there is little information about function. Images from positron emission tomography (PET), single photon emission tomography (SPECT), and functional magnetic resonance imaging (fMRI) give functional information; anatomy is, however, poorly visible. The same equipment can sometimes produce anatomical images and functional images, as is the case with the MR camera. There are also scanners that combine two very different acquisition modes such as CT and PET in the same device. For readers interested in more detailed descriptions about tomographic modalities other literature is available, see, for instance, [55].

At the Centre for Image Analysis, we currently work with image data acquired using MRI, fMRI, magnetic resonance angiography (MRA), CT, SPECT and PET. In addition to the different kinds of modalities, a scanner may support several acquisition methods of acquiring the data, e.g., T1, T2, and inversion recovery (IR) using MRI.

As it is not an easy task for the physician to imagine how the combined information from different modalities could be interpreted, a computerised brain atlas (CBA) [35], [102] has been developed. See Section 1.4 for a description of the brain atlas project.

1.1.1 Magnetic Resonance Imaging (MRI)

Magnetic resonance imaging (MRI) is a widely employed imaging technique that can be used for both anatomical and functional images. In a strong magnetic field, atoms with an odd number of nucleons have the magnetic moment (also denoted as spin) of the atom nucleus aligned with the direction of the field. This principle is used in MRI. A short radio frequency pulse is transmitted, which alters the direction of the net magnetic moment. The frequency has to match the frequency of the protons that it is processing. The pulse excites the protons to a higher energy state which they leave as soon as the pulse is switched off. The spins return to their equilibrium state and electromagnetic radiation is emitted. This takes some time, which is referred to as the relaxation time. The two relaxation times measured are referred to as the T1 and T2 relaxation times, respectively.

The relaxation times are different for different kinds of tissue, which gives different intensities in the image. These slices are registered together; the methods for image registration are described later in this thesis. T1 is the longitudinal relaxation time: the time it takes for the proton magnetic moment to reach its previous equilibrium state in line with the magnetisation axis of the constant external magnetic field. This relaxation depends on how the protons exchange energy with their surroundings and that is in its turn dependent on the tissue type. T1 is the time it takes the excitation to return to 63% of its original value.

T2 is the transversal relaxation time: this depends on internal dephasing factors and the intensity is reduced. During the dephasing process the protons lose their synchronicity and start spinning at different rates. When the proton spin returns to its aligned axis, the amplitude of the signal decays exponentially to zero. T2 is the time it takes for the signal to return to 37% of its original value.

A T1-weighted image is quite different from a T2-weighted image, see Figure 1.4 for the coronal slice of an MRI T1-weighted image and the corresponding MRI T2-weighted image of a brain. There is a lot of ongoing research on new pulse sequences, aimed at producing either different kinds of characteristics or faster acquisition times while preserving the same characteristics.

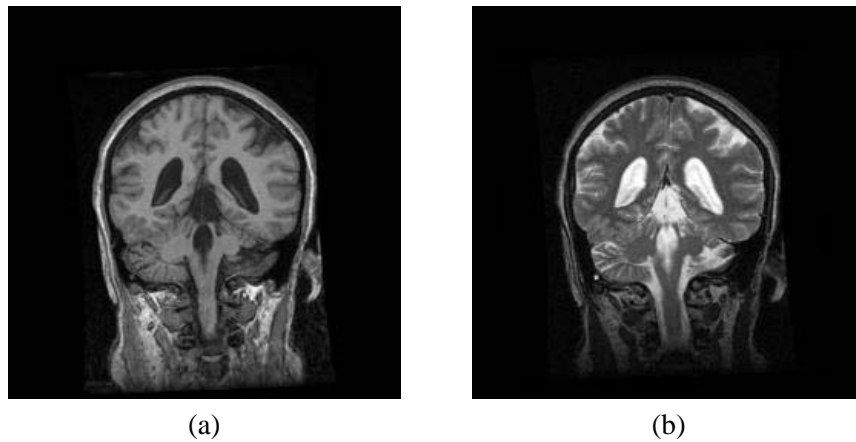


Figure 1.4: a) T1-weighted coronal slice. b) T2-weighted coronal slice corresponding to the T1-weighted slice.

1.1.2 Computed Tomography (CT)

Computed tomography (CT) is based on the measuring of X-rays transmitted through the object from several different angles. The X-rays originate from a rotating X-ray source inside a ring around the object and the detectors are located on the opposite side of the object. An image slice is then reconstructed and a 3D volume is built up by moving the X-ray source and reconstructing more slices. There are different ways to move the X-ray source. The X-ray source can rotate in a ring that is moved or on a spiral, also called helical scanning. There are also a few different ways the X-rays are emitted and the corresponding set of detectors are placed. The most common are cone-beam and fan-beam. There are several different reconstruction algorithms available, but the conventional algorithm is based on filtered-back projection.

1.1.3 Positron Emission Tomography (PET)

Positron emission tomography (PET) is used for functional imaging. PET is based on the detection of radiation from a radioactive positron-emitting isotope or tracer administered to the patient. Positrons interact with electrons, resulting in the emission of two anti-parallel photons. If two photons are detected almost simultaneously by two detectors opposite each other, the position for the reaction causing the photon emittance can be determined. The detectors in the PET camera are positioned in a ring around the patient. The resulting image is reconstructed from a large number of photon detections and shows the distribution of the radioactive isotope in the patient. The isotopes or tracers can be designed to bind to specific molecules, which allows PET to be used in a broad variety of functional studies. In Figure 1.5, a PET image is shown.

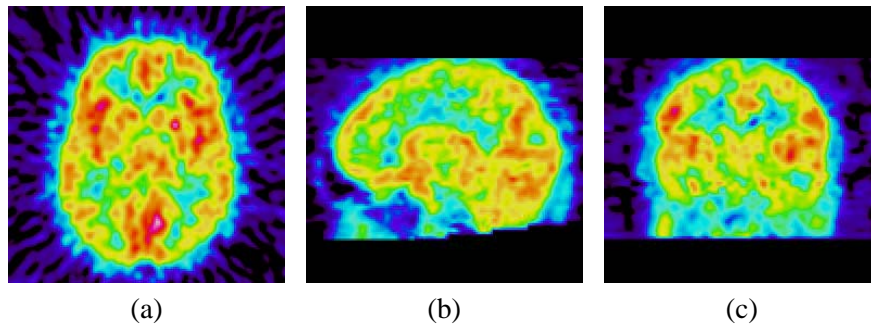


Figure 1.5: An activation from a PET image of the brain, showing transaxial, sagittal, and coronal slices. See page 65 for a colour version of the figure.

1.1.4 Single Photon Emission Computed Tomography (SPECT)

Single Photon Emission Computed Tomography (SPECT) is also used for functional imaging. SPECT is based on the detection of gamma photons from a radioactive isotope inside the patient. This isotope is administered as a radiopharmaceutical substance. The main difference, compared to PET, is that SPECT only detects one photon. Because of this, a collimator is placed in front of the detectors in order to allow only photons that are in a narrow angle from the object to be detected. Still, the image resolution will typically be lower than for PET. The algorithm for reconstructing the image is similar to CT. In Figure 1.6, a SPECT image is shown.

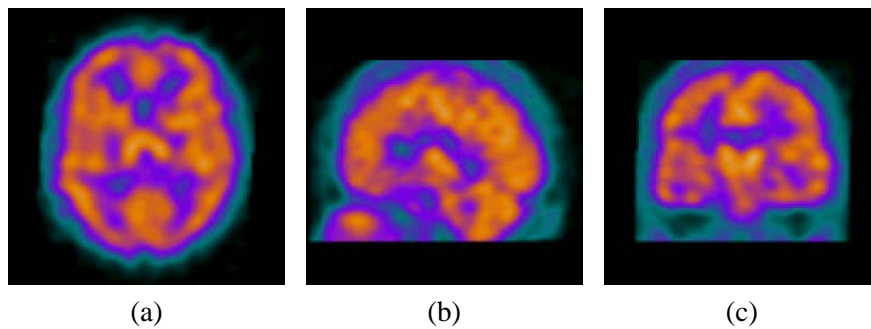


Figure 1.6: An activation from a SPECT image of the brain, showing transaxial, sagittal, and coronal slices. See page 65 for a colour version of the figure.

1.2 Registration

In order for work on several images of the same object to be possible, the anatomical location of the pixel or voxel in one image must correspond to the same anatomical position in the other image. The images need to be registered

or matched, that is, translated and rotated to fit on top of each other, for intra-person examinations. For inter-person examinations the registration algorithm must account also for shape differences. Hence, a more complex transformation is needed. There are several different approaches to matching [67]. The registration most often follows the same general steps, iterated until convergence is reached according to some criteria. The first step is that a transformation is applied to the image to be matched. The next step involves evaluating a similarity measure from the reference image and the image to be registered. If convergence is not reached, a new set of transformation parameters is selected and the procedure repeated.

1.3 The Image Processing (IMP) Environment

In this thesis, the development platform IMP (Image Processing) [75] has been used for the implementation of the algorithms described in Papers III and V–IX.

The program IMP has been developed at the Centre for Image Analysis, Uppsala University, Sweden, and is being used in several different projects from quantitative shape analysis for example [11] and segmenting medical images [85], [50], [111] to determining crop from satellite images [81]. IMP is a general image analysis software for five dimensional image data (x, y, z, t, b) . The five dimensions are spatial dimensions (x, y, z) , the time dimension (t) , and the spectral or bandwidth dimension (b) , which can be used for standard colour images with red (R), green (G), blue (B). The software runs on most UNIX systems. It is possible to add new functions to the program using C or C++ and to automate time-consuming multi-step procedures using the built-in macro language.

1.4 The Computerised Brain Atlas (CBA) Project

The Computerised Brain Atlas (CBA) has been the main tool used in Papers II and IV. In Paper I, the implementation of the algorithm was done in a stand-alone environment and the 3D-display was created using CBA and also the 3D visualisation software developed prior to the integration with the CBA software. In Papers III, V, and VI most data sets were in the CBA image format and CBA was also used for displaying the segmented volumes. The implementation was, however, initially done in the IMP environment.

The brain atlas project was initiated by professor Torgny Greitz at the Department of Neuroradiology at the Karolinska Hospital in the mid-1970s. In collaboration with the Department of Physics at the University of Stockholm,

a cryosectioned brain was digitised and computer programs were developed for creating an atlas data base.

The atlas structures in the CBA were identified from the digitised photos of the cryosectioned brain, and created using anatomical information found in literature [35]. The definition and classification of the anatomical structures and divisions are in agreement with standard textbooks of anatomy. The nomenclature is that of the *Nomina Anatomica* of 1965. The boundaries of the cortical cytoarchitectonic areas ("Brodmann areas") have been determined using information from several sources. The use of only one individual to create the data base does not invalidate the atlas as a standard, because all relevant gross features should be present. There are about 400 different 3D structures in the CBA data base.

The brain on which this atlas was based exhibited several unusual aspects, which increases the demand on the transformations that are used to adapt the atlas to an individual brain. Statistics, as well as experience, have shown that it is extremely difficult to find a specific sample that is "normal" in most ways. Because of this, new atlas structures are being developed, which is based on a mean of co-registered MRIs, several new regions have been drawn, including blood supply areas and inner brain structures. The utilisation of structures drawn for the original atlas are in the planning. These old structures will be registered to match as well as possible and then altered to adapt to the mean MRI brain. This new brain atlas was one of the reasons that a segmentation tool needed to be implemented. There is a drawing program for the UNIX version (CBA ver. 3.2) that has been used to develop the structures drawn on the mean brain.

As the original program was developed, the first results were reported in 1982; different aspects on the usage of the first system are found in [8], [7]. In 1991 it, was decided that the CBA program needed a substantial update. Further development of the brain atlas was done in collaboration between the Centre for Image Analysis and the Karolinska Hospital and University of Stockholm. The program was completely rewritten in ANSI-C using X11 and OSF/Motif for display [101].

The first version implemented for use with Windows 9x/NT version 4.0 from 1995 was still written in C. The current version (ver. 5.0) has an object-oriented design and is written in C++, [63]. The development platform is Microsoft Visual C++ and the program uses the Microsoft Foundation Classes (MFC) library for the graphical user interface (GUI) programming. This version also includes 3D visualisation of various kinds, see Figure 1.7. The version of CBA (ver. 4.0) that has been used at hospitals only has 3D visualisation of data that have been converted to a geometric format. See Figure 1.8 for an example of activated areas combined with structures from the brain atlas database. For an explanation of the 3D visualisation in CBA, see Chapter 3.

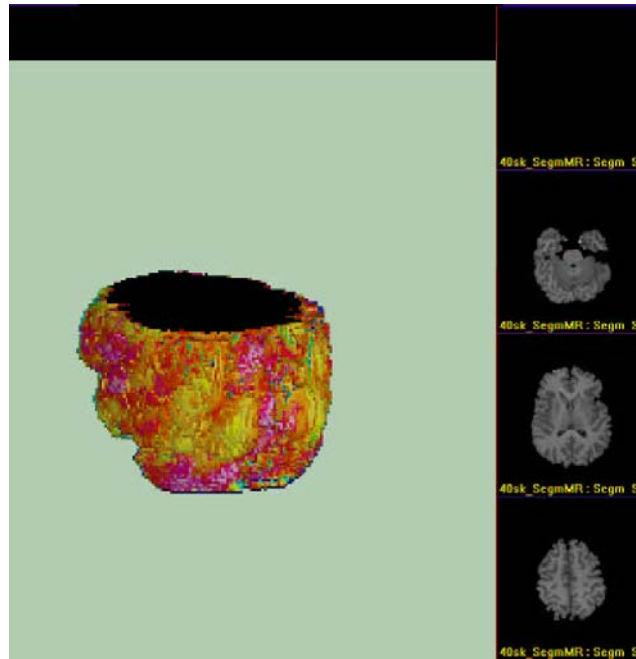


Figure 1.7: A 3D visualisation in CBA 5.0. See page 65 for a colour version of the figure.

1.5 The BRAINS2 Software

In Papers VI, VII, and IX, data in BRAINS2 format has been used. BRAINS2 has also been used for visualisation purposes. The BRAINS2 [65] program is from the Mental Health Clinical Research Center, University of Iowa College of Medicine and Hospitals and Clinics, Iowa City, USA. BRAINS2 is a software package for analysis of images of the human brain. There are tools for segmentation and tissue classification. The BRAINS2 package was developed out of the BRAINS (Brain Research: Analysis of Images, Networks, and Systems) package. The program is written in C and the OpenGL is used for visualisation. It contains an image processing toolbox, and tools for registration and manual and automatic delineation of structures.



Figure 1.8: Activated regions, visualised together with a model of the ventricles. A surface rendering method has been used.

Methods Used in Brain Segmentation

2.1 Grey-level Morphology

Morphology usually denotes a branch of biology that deals with the form and structure of animals. Mathematical morphology is a tool for extracting image components that describe and represent a shape. The main references on mathematical morphological image processing are the books by Serra [91], [92]. A short introduction can be found in [32]. The morphological techniques have evolved from set theory, but a detailed explanation of this using set theory is outside the scope of this thesis, instead a verbal description will be given.



Figure 2.1: a) Binary structuring element with radius r , viewed from above. b) Binary structuring element viewed from the side. The y dimension is intensity (either 0 or 1 for binary objects).

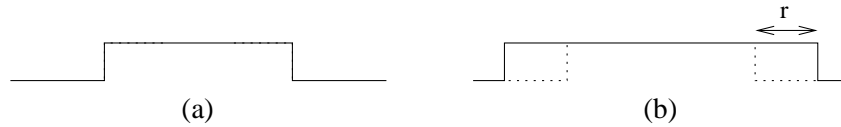


Figure 2.2: a) Original binary image viewed from the side. b) Image dilated with the structuring element from Figure 2.1.

Morphology can be defined on binary as well as grey level images. Binary erosion consists of a structuring element traversing throughout the image and eroding half of its thickness from the object. If a 3×3 structuring element



Figure 2.3: a) Grey-level dilation structuring element with radius r , viewed from above. b) Grey-level dilation structuring element viewed from the side. The y dimension is intensity.

is applied to a 2D image then all border pixels are deleted. If at least one of the pixels in a 3×3 neighbourhood is a background pixel, then the pixel corresponding to the pixel in the middle of the 3×3 neighbourhood is removed. The same holds for dilation, but instead a layer one pixel thick is added to the object in the image.

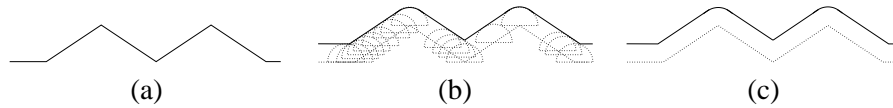


Figure 2.4: a) Original grey-level image viewed from the side. b) Image dilated with the structuring element from Figure 2.3. c) Result of the dilation.

When grey-level morphology is used, an extra dimension is added to the structuring element, the height. Besides the spatial dimensions, an intensity dimension is also used. The structuring element can be of arbitrary shape: in the examples in Figure 2.1 to Figure 2.7 disc-shaped structuring elements are used. The binary structuring elements have either the height 0 or 1. Grey level structuring elements have a height that depends on where on the half sphere they are. In this description the intensity of the image is considered to signify the “height” of the image. A dark area is a valley and a bright area is peak.

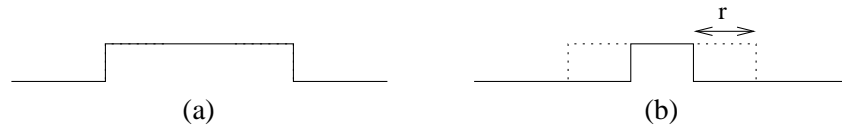


Figure 2.5: a) Original binary image viewed from the side. b) Image eroded with the structuring element from Figure 2.1.

When a binary object is dilated, the object expands with the amount r if the structuring element from Figure 2.1 is being used, according to Figure 2.2. On grey level objects the structuring element in Figure 2.3 passes over the



Figure 2.6: a) Grey-level erosion structuring element with radius r , viewed from above. b) Grey-level erosion structuring element viewed from the side. The y dimension is intensity.

whole object and the maximum value is selected at each point, according to Figure 2.4. The peaks are rounded off, but the valleys remain sharp.

When a grey level image is dilated, the resulting image is brighter, the darker details are reduced. The size of the details is approximately the same as the dimensions of the structuring element, see Figure 2.8. The opposite is true for erosion. In the segmentation algorithms in this thesis a cubic structuring element of size $3 \times 3 \times 3$ has been used. It is the maximum value in the $3 \times 3 \times 3$ neighbourhood that is stored in the output volume.

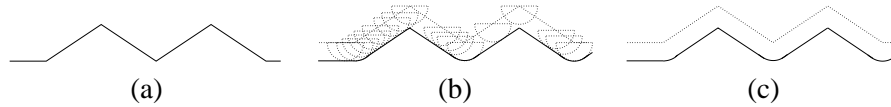


Figure 2.7: a) Original grey-level image viewed from the side. b) Image eroded with the structuring element from Figure 2.1. c) The result of the grey-level eroding.

In erosion of a binary object, the object shrinks with the amount r , according to Figure 2.5. On grey-level objects the structuring element in Figure 2.6 pass over the whole object and the minimum value is selected at each point, according to Figure 2.6. The valleys are rounded off, but the peaks remain sharp. The resulting of grey level erosion is darker and the bright details are reduced. The erosion in the segmentation algorithms also use a cubic structuring element of size $3 \times 3 \times 3$. It is the minimum value within the structuring element that is stored in the output volume.

Several segmentation methods use binary morphology. We have not found any segmentation methods that employ grey-level morphology for use on the cortex. The grey-level morphology is a strong tool since it uses structuring elements to find specified neighbour information. Dilation enhances the bright areas in the image and is similar to growing the area when using binary morphology. Erosion enhances the dark areas in the image, this is also similar to the binary case. Binary erosion cannot create cavities that are not present, but when grey-level erosion is combined with thresholding, new gaps can occur.

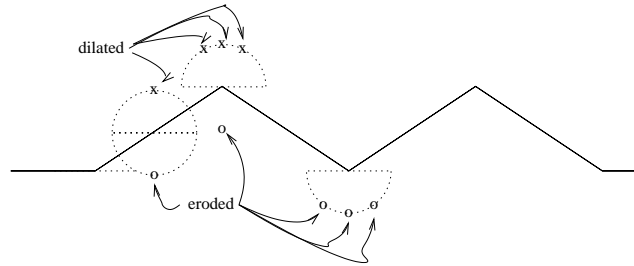


Figure 2.8: This is what the new intensities would be after dilation and erosion.

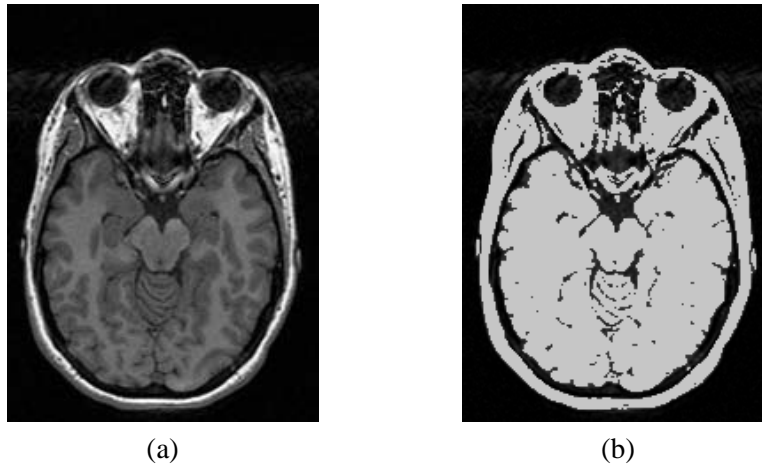


Figure 2.9: Thresholding slices. a) A transaxial slice. b) What the threshold algorithm detects.

This is why it is possible, by using grey-level morphology as an aid, to break connections between tissues, which would be impossible when operating only on the binary mask. If the binary bridge could be broken, the mask may be altered so that it is no longer possible to reconstruct the original shape. See Figures 2.9 and 2.10 for examples of how grey-level morphology works. The results from automatic thresholding are also shown. In Figure 2.11 there is an example of how the grey-level erosion may look. In these grey-level morphology operations no new grey-levels are introduced, since the structuring element operates on a sorted list of the neighbouring voxels (or pixels in the 2D case).

The grey-level erosion can remove bands of noise in the volume if high values are not present in large neighbourhoods. In the case where at least one voxel in a $3 \times 3 \times 3$ neighbourhood is at the real background level, the grey-level erosion can remove the noise. See Figure 2.12 for an example of such an event. Without grey-level erosion, the 2D binary erosion would be able to break the connection to the outer tissue.

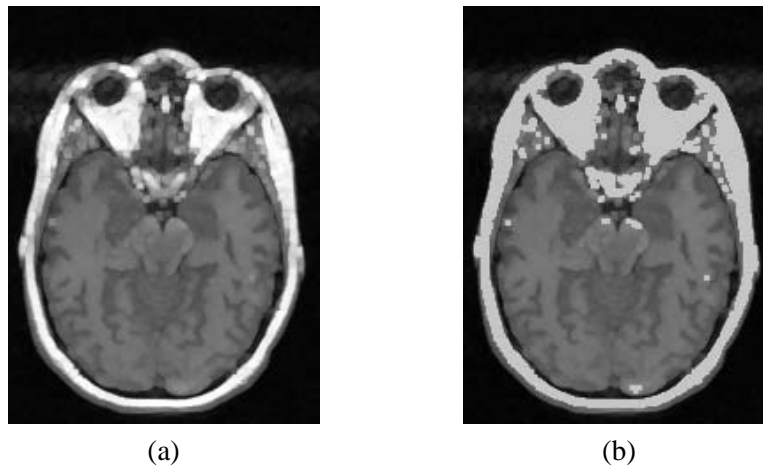


Figure 2.10: Thresholding slices. a) A grey-level dilated slice. b) The bright area that the threshold algorithm detects.

2.2 Segmentation of the Cortex from MRI

2.2.1 A Short Survey of Segmentation Techniques Used to Segment the Cortex

There are a few different approaches to segmenting MRI. The most used technique is still manual segmentation, although it has severe shortcomings: for example, it requires a substantial amount of background knowledge of the objects to be segmented. Manual segmentation is also very time consuming, which means it is costly. Maybe the most problematic aspect is that it is not reproducible, since it involves subjective decisions. Another approach that is also common is based on automatic grey-level thresholding [98], [59], [12]. These techniques have some common steps. A histogram is determined, from which the threshold levels are determined to produce a binary mask. Then binary morphology, sometimes combined with expert knowledge, is applied to the binary mask to get a new mask that hopefully will be equivalent to the cortex. The problems with these methods include their sensitivity to shading effects.

There are also methods based on region growing [116], [48], [94]. One of these methods [116], is an interactive method, where the seeds are planted manually. Another of these methods is an automatic iterative method [48]. These methods also use binary morphology to break connections to non-brain tissue.

Furthermore, there are methods that have a more statistical approach [57]. Similar to these are methods that utilise artificial neural networks [114], [115]. These methods require both T1- and T2-weighted MRI-data sets to work. Some statistical methods employ only one MRI scan, using statistical char-

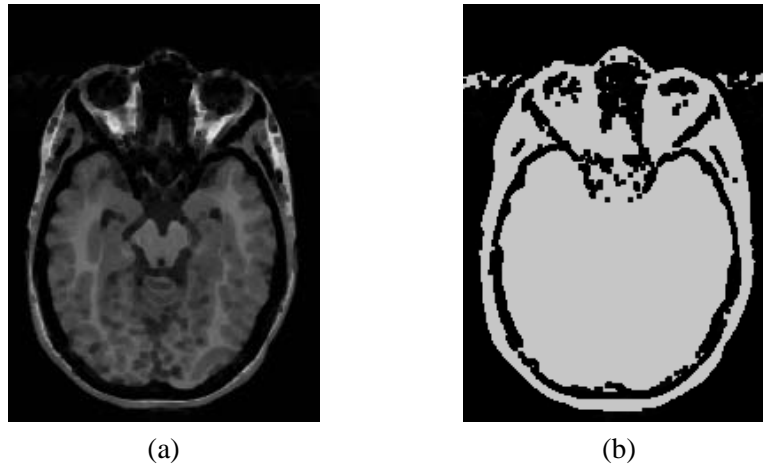


Figure 2.11: Thresholding slices. a) A grey-level eroded slice. b) The areas that the threshold algorithm detects.

acteristics of the histogram [73], [88].

There are methods employing active contours [14], [4]; those have models of physical forces that pull the boundary into the right position. Finally, a different approach is using active shape models [18]. An active shape model is a parametrically deformable shape model algorithm designed to find the brain boundary.

There are at least three reasons why a simple thresholding technique and connected component labelling are insufficient: there is always some shading because of artefacts in the RF magnetic field created by the coils in the camera, outer structures are often linked to the brain tissue, and noise, imaging artefacts, and sometimes poor distribution of the grey-levels increase the difficulties to distinguish brain tissue from non-brain tissue. This is not a complete survey of MRI segmentation methods. A detailed comparison of common methods is not possible within this thesis, but the reader interested in knowing more about other segmentation methods may consult the various papers in the field, see e.g. [15] for a review.

2.2.2 An Overview of the Progress of our Grey-level Morphology-Based Segmentation

The segmentation processes groups of voxels that are intra-brain to get coherent volumes that can be used in quantitative volumetric analysis, or in morphological analysis, as well as for visualisation. Segmentation of the cortex is useful not only for providing a model for functional studies, but also for quantitative analysis of brain structures to be used as a tool for diagnostics.

The segmentation algorithms are described in detail in Paper III, Paper V,

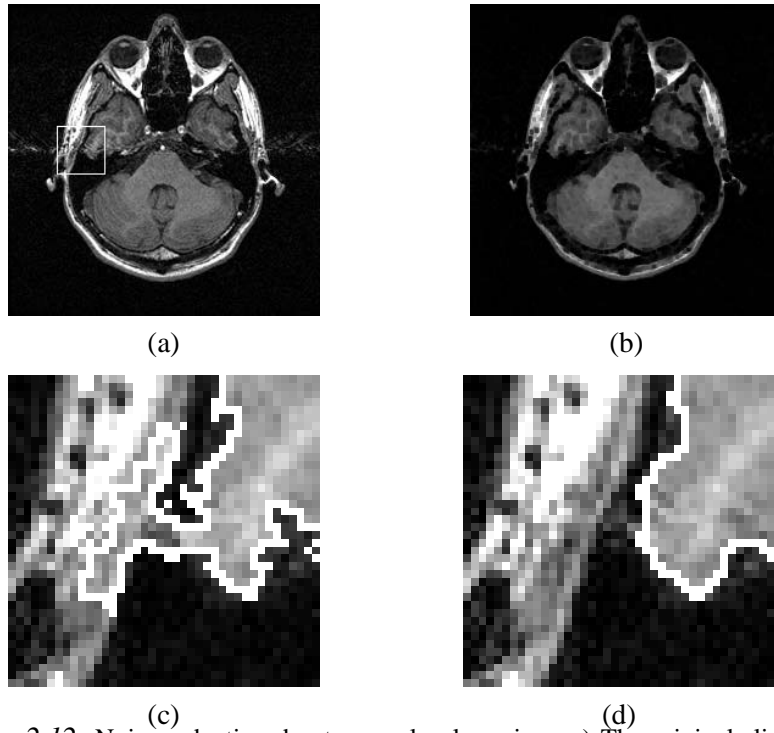


Figure 2.12: Noise reduction due to grey-level erosion. a) The original slice with noise present. b) Noise has been eroded significantly. c) Segmentation result without using grey-level erosion. d) Segmentation result using grey-level erosion.

and Paper VI. The papers recount progressive development over time. The algorithm in Paper III was developed for segmenting transaxially acquired MRI. The algorithm in Paper V is more advanced, as it can segment MRI taken in transaxial and sagittal directions. The algorithm in Paper VI is the most advanced, as it can segment MRI acquired in all three directions, that is transaxial, sagittal, and coronal directions.

Earlier we have mostly encountered data sets where the slices were transaxial. To cope with sagittal data the background had to be removed, otherwise it was very difficult to make the segmentation algorithm robust enough. An advantage with this, compared to the original algorithm in Paper III, is that the new algorithm in Paper V and VI is less sensitive to poor image quality. This is due to the background causing no interference, since it is not valid terrain for brain tissue. To remove the background the volume is grey-level dilated and thresholded, keeping the brightest areas. The thresholding is performed on kernel density estimates (continuous histogram) [60], [87], [80]. The improved algorithm even produced a quite successful result on an MRI that was reformatted to 79×95 with 68 slices, although the difference between the sulci

and the gyri was less than perfect due to smoothing effects that occurred when the volume was down-sampled.

2.2.3 An Overview of our Grey-level Morphology-Based Segmentation

The automatic segmentation method is based on general anatomic knowledge of the brain seen from three different directions, transaxial, sagittal and coronal. Grey-level morphological operations on the MRI data, and also binary morphological operations on thresholded data from the original MRI data set are used. The thresholding employs an automatic histogram thresholding technique. There are also logical operations involved in order to ascertain that only pixels that are within a mask are kept. The method is a 3D method that uses 3D erosion and 3D dilation of grey-level data, and 2D erosion and 2D dilation of binary data. The information propagates between consecutive slices to avoid growing beyond the border of the desired volume of the brain.

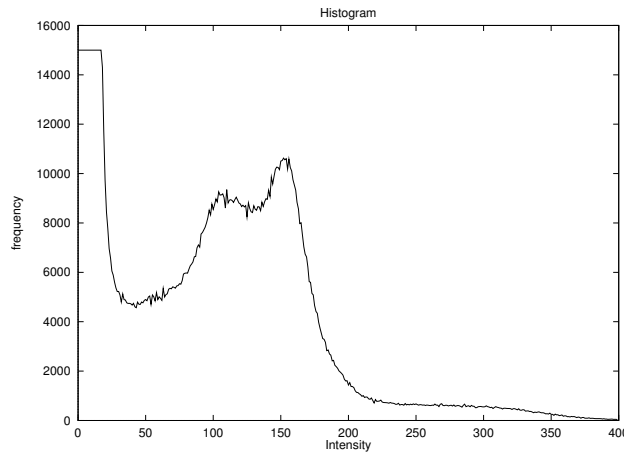


Figure 2.13: Grey-level histogram of a complete 16-bit 3D MRI data set with normal resolution in grey-levels. (The histogram was cut at frequency 15,000 and grey-level 400.)

Our approach is similar to the other histogram-based methods. The grey-level morphology that is used in conjunction with binary morphology makes it possible to break stronger connections between the brain surface and objects that are not on the surface. For an example of the grey-level distribution in an MRI data set, see [Figure 2.13](#).

The algorithms in the thresholding procedure are visualised using flow-charts. A description on what the different arrows represent can be seen in [Figure 2.14](#).

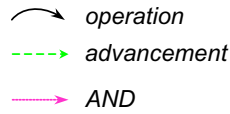


Figure 2.14: Description of arrows used in the flow-charts.

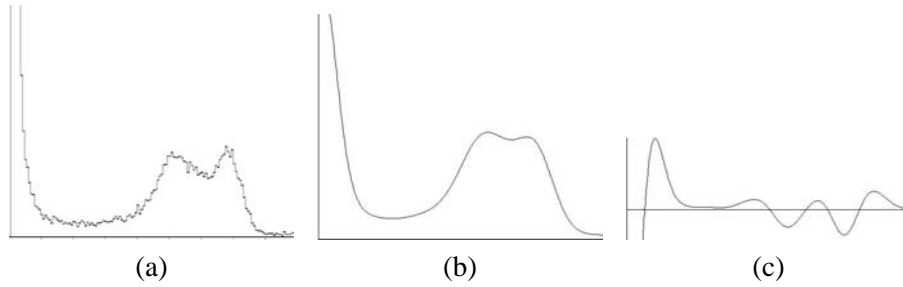


Figure 2.15: a) Grey-level histogram of a mid slice in a 3D MRI data set. b) KDE and c) second derivate plot of the same slice.

The thresholding is performed on a continuous histogram (kernel density estimates (KDE)) [60], [87], [80] from which the second derivate is calculated. Then the four highest maxima are determined (not counting the initial peak that corresponds to the background). Figure 2.15 shows the histogram and the continuous histogram with the second derivate for a mid slice in a 3D MRI data set. There is, of course, a difference if the histogram thresholding is applied on the whole volume or only on the middle slice. In Paper III only the middle slice is used, since there are not as many irrelevant structures that may affect the thresholds: for instance, there are not many very bright areas that represent fat tissue. In Figure 2.16 the thresholding of brain matter is shown.

Paper V is an improvement on Paper III, since the segmentation capabilities are extended further to handle data acquired sagittally. For sagittal data, it was necessary to remove the background to make the segmentation algorithm robust enough. As stated above, we had encountered mostly data sets where the slices were transaxial.

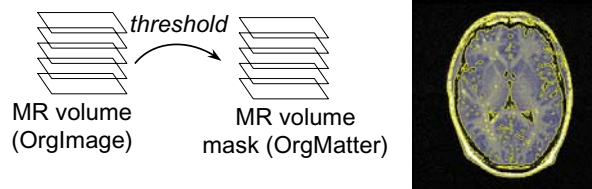


Figure 2.16: Preparation step (OrgMatter).

In the case of sagittal data we use a slice one fourth into the volume. When an average from the whole volume is used, then more of the brighter parts of the brain are taken into account. We have also tried to threshold each slice based on its own histogram, but on some slices this fails completely.

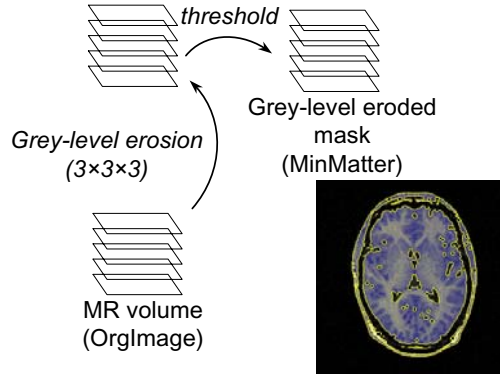


Figure 2.17: Preparation step (MinMatter).

In Paper III only a grey-level eroded volume was used to reduce bridges between the brain tissue and surrounding tissue types, see Figure 2.17. In Paper V and Paper VI there are two additional grey-level volumes that are produced through grey-level erosion and grey-level dilation. The eroded volume minimises connections to non-brain tissue. The dilated volume enhances background fat, tissue that should not be included in the brain during the segmentation process.

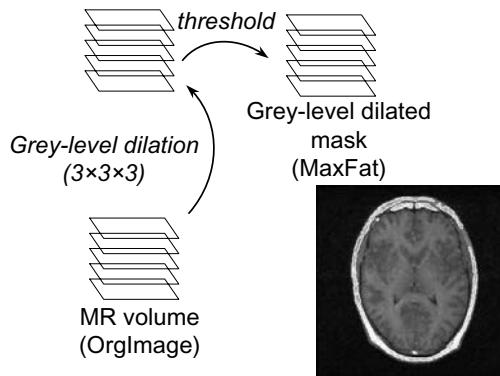


Figure 2.18: Preparation step (MaxFat).

Paper V and Paper VI describe in detail how the algorithm works. To remove the background, the volume is grey-level dilated and thresholded keeping the brightest areas, see Figure 2.18. These areas and the background from the original volume are then not allowed as brain tissue.

The segmentation algorithm in Paper III uses a start slice and propagates

the information to consecutive slices. In Paper V, when sagittal volumes are segmented, two start slices are used due to the difficulties with the border between the two hemispheres. In Paper VI, when coronal volumes are segmented, again, two start slices are used because the brain is divided into several regions.

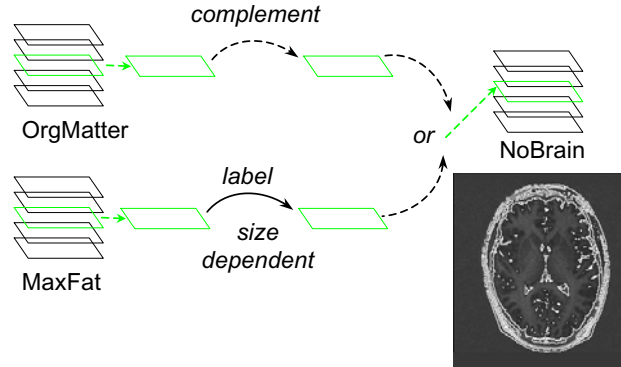


Figure 2.19: Background algorithm (start).

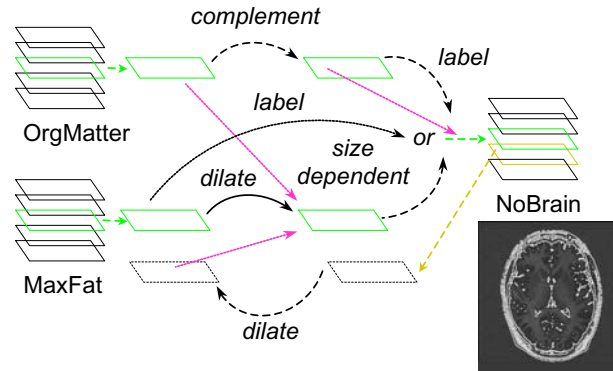


Figure 2.20: Background algorithm.

First the background is segmented, then the brain cortex. The algorithm uses binary morphology, conditions from the background, the thresholded original volume, and grey-level eroded volume to segment each slice. Figure 2.19 and Figure 2.20 show flow-charts of the background segmentation.

When the background is segmented, the start slice is segmented, or the two start slices if sagittal or coronal segmentation is used. See Figure 2.21 for a flow-chart of the algorithm for the start slice.

The actual segmentation of the brain uses propagation of information from previously segmented slices. The algorithm can be seen in Figure 2.22. Figure 2.23 demonstrates how the information propagates throughout the volume.

Figure 2.24 shows how the result might look when segmenting data ac-

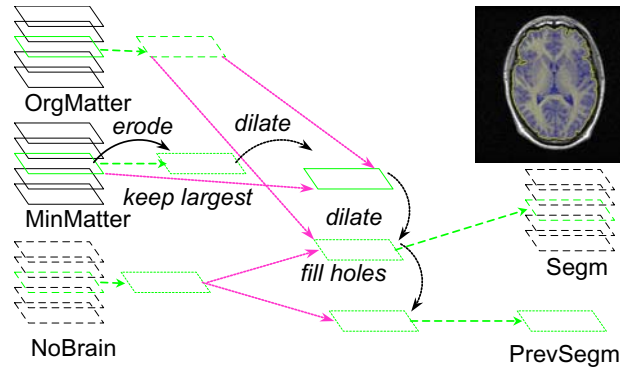


Figure 2.21: Start slice.

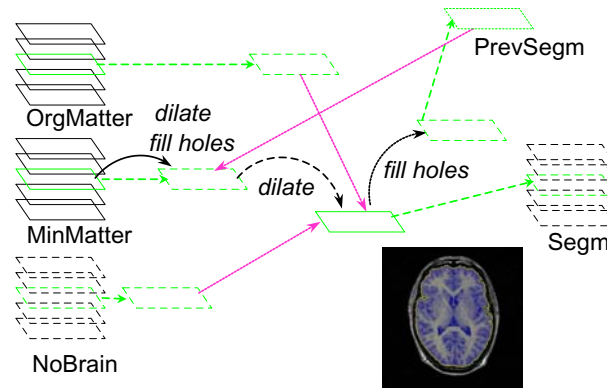


Figure 2.22: Segmentation algorithm.

quired in the three different directions.

Manual editing is undesirable since it introduces subjectivity. It is possible to restart the algorithm at a selected slice, after correction, if the segmentation is less than satisfactory.

The result of the segmentation can be viewed in 2D slices as well as in 3D projections. For an example of a volume segmented with the algorithm see Figure 2.25.

The automatic thresholding algorithm only encountered difficulties when the intensity resolution was very poor. In Figure 2.26 there is an example of a histogram of an image with few different grey-levels.

2.3 Segmentation of the Hippocampus from Multivariate MRI

The hippocampus is located in the medial temporal lobe of the human brain and is considered part of the limbic system; it is divided into three parts: head,

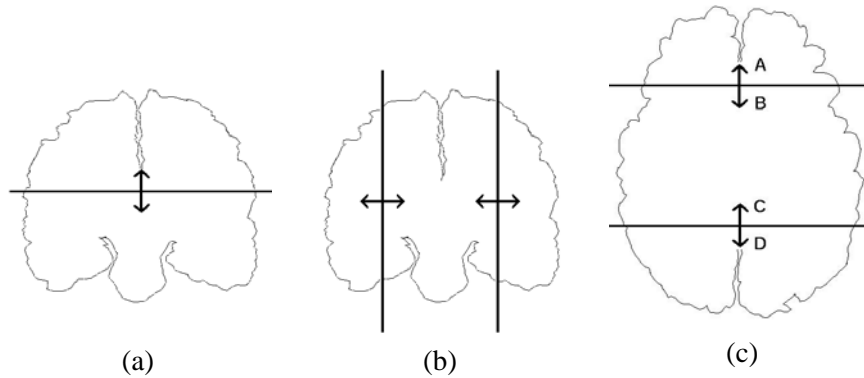


Figure 2.23: How the algorithm propagates on: a) A transaxial volume. b) A sagittal volume. c) A coronal volume.

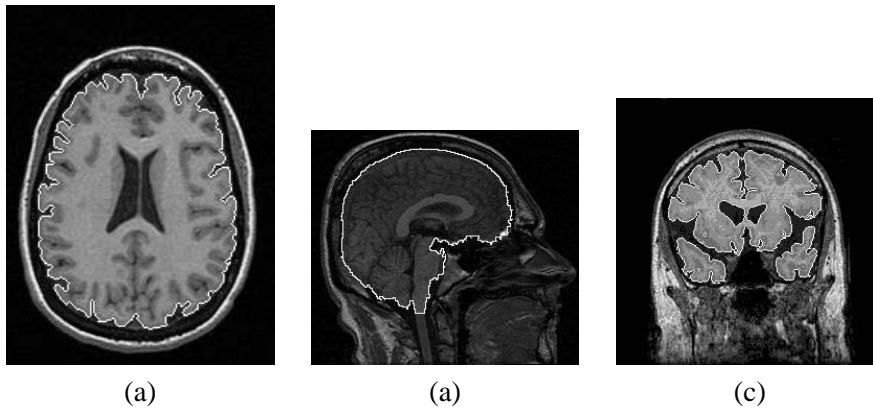


Figure 2.24: Segmented slices. a) A transaxial slice. b) A sagittal slice. c) A coronal slice.

body, tail. The hippocampus is a relatively difficult structure to segment automatically due to its bent shape. The volume of the hippocampus is studied for example in schizophrenia research.

There are several different methods describing how to segment the hippocampus. Brain atlases of some sort can be used to aid the segmentation [45], [23]. Active shape models (ASM) or point distribution models (PDM) have been used [56]. Regional fluid registration has also been used for segmentation of the hippocampus [19].

A part of the hippocampus that is easy to delineate is the most lateral part of the hippocampus, when viewed in the sagittal plane. The head and tail of the hippocampus appear on medial slices and become increasingly more difficult to delineate and separate from surrounding structures of the brain in the MR images. See Figure 2.27 for a 3D view of the shape of the two hippocampi and a segmented transaxial slice.

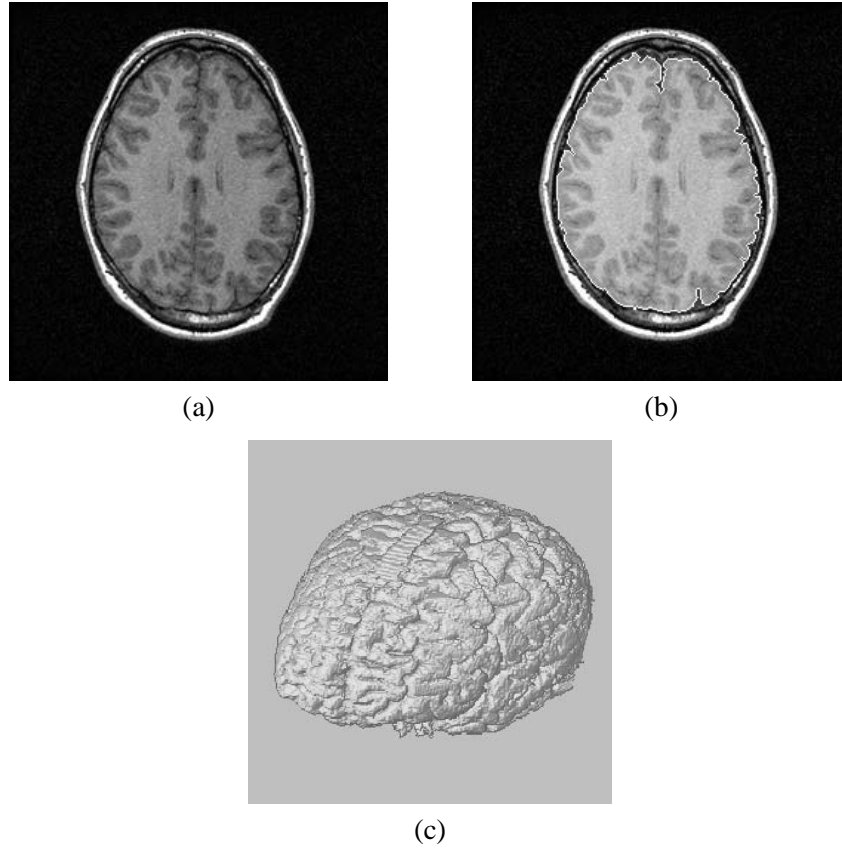


Figure 2.25: Visualisation of segmented volume. a) The original slice. b) The segmented slice with the ROI appearing as lighter grey-shade. The edges are shown as a white outline. c) The segmented volume shown as a ray-casted image.

The segmentation uses three MR data acquisition protocols, T1-weighted, T2-weighted, and a continuously classified stereo image, to delineate the hippocampus. Prior to the segmentation, the T1-weighted and T2-weighted volumes are registered in the AC-PC line in BRAINS2 and classified. A bounding box is manually selected and the ANN segmentation in BRAINS2 is performed using the classified image. This segmented hippocampus is then used as input to the grey-level morphology-based segmentation.

The ANN seems always to detect too small an amount of the hippocampus. One reason for this undersegmentation might be that a classified image is used, which may not contain all grey-level information that is necessary for a correct segmentation of the hippocampus. It seems as if this ANN segmented volume never extends outside the hippocampus and therefore no external tissue is included. The effort has been directed at extending the boundaries found by the

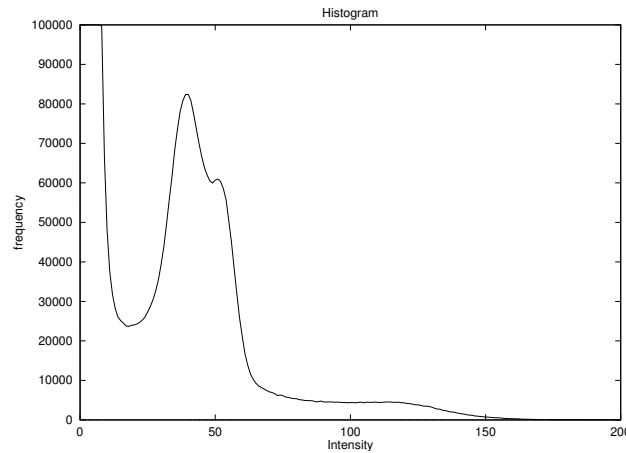


Figure 2.26: Grey-level histogram of a complete 16-bit 3D MRI data set with poor resolution in grey-levels. (The histogram was cut at frequency 100,000 and grey-level.)

ANN segmentation into a more correct segmentation of the hippocampus. It would be troublesome for the grey-level morphology-based segmentation if the hippocampus segmented by the ANN would include tissue that is not regarded as belonging to the hippocampus.

In both Paper VII and Paper IX, the T1-weighted and T2-weighted MRIs are grey-level eroded and dilated. For a description of the arrows used in the flow-charts see Figure 2.28. The foreground is found by thresholding the grey-level eroded T1-weighted MRI. The lateral part of the hippocampus is segmented using the previously segmented hippocampus and the T1-weighted and T2-weighted MRIs as well as the segmented possible hippocampus foreground, See Figure 2.29 and Figure 2.30. In Paper IX, the hippocampus head and tail are segmented separately using the T1-weighted and T2-weighted MRI, the laterally segmented hippocampus, and the foreground, see Figure 2.31 and Figure 2.32. The algorithm is also applied on the grey-level eroded and dilated MRIs and the result is combined, using an AND operation. The algorithm is applied in all three directions and combined using an OR operation. In Paper VII, the result from the lateral segmentation algorithm is used as input to the final segmentation combined with T1-weighted and T2-weighted MRI and the result from the foreground segmentation. In Paper IX, the result from the hippocampus head and tail is used instead of the result from the lateral segmentation algorithm. See Figure 2.33 for a flow-chart of the final segmentation algorithm. This algorithm is also applied on grey-level eroded and dilated MRIs, in all three directions, and the results from all these are combined using an AND operation.

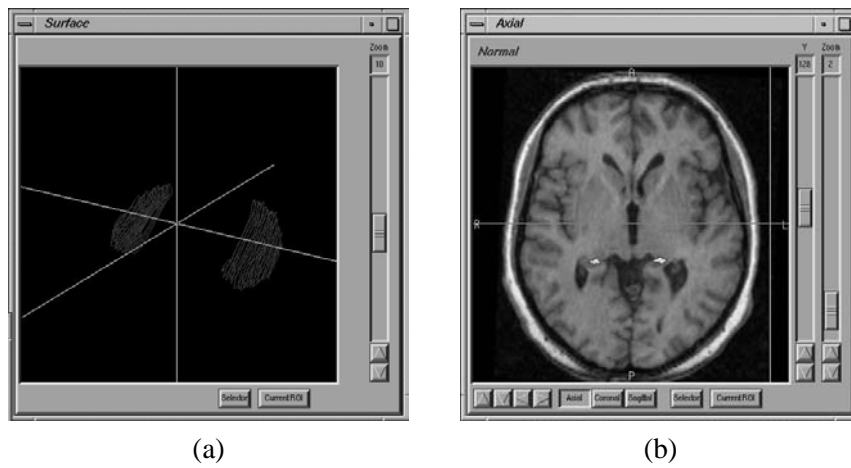


Figure 2.27: Segmented hippocampi viewed as contours. a) Contours in 3D. b) The hippocampus displayed as contours in the axial plane, surrounding the hippocampi which are the two white areas.

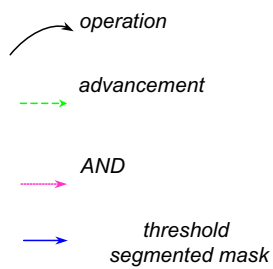


Figure 2.28: Description of arrows used in the flow-charts.

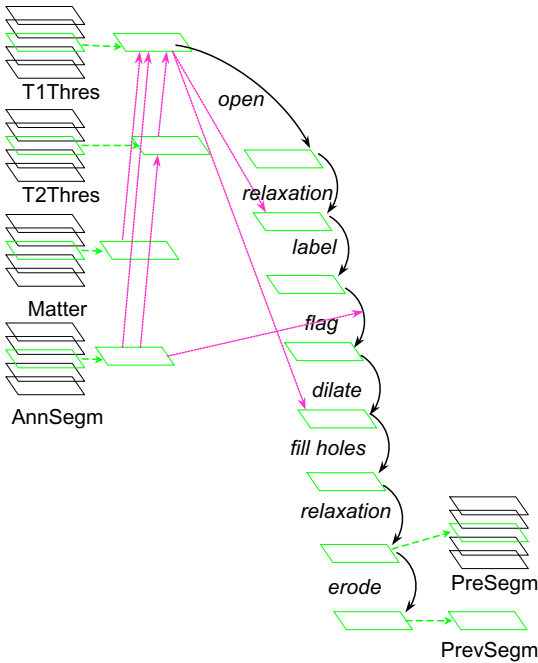


Figure 2.29: Lateral part of the hippocampus in sagittal slices, start slice.

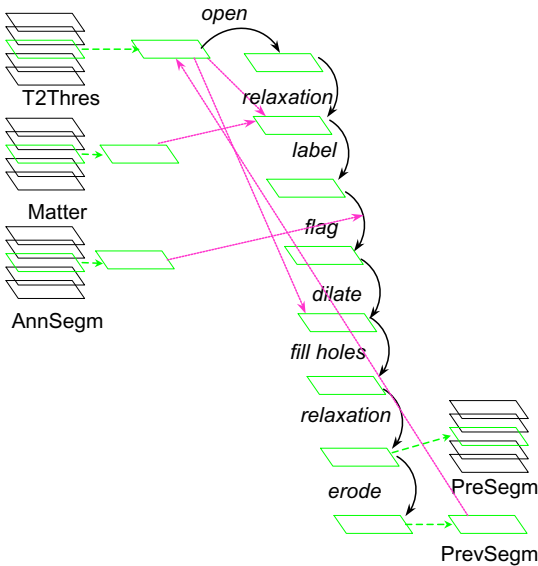


Figure 2.30: Lateral part of the hippocampus in sagittal slices, traversing volume.

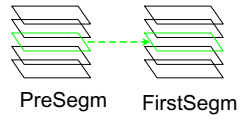


Figure 2.31: Hippocampus head and tail segmentation algorithm, start slice.

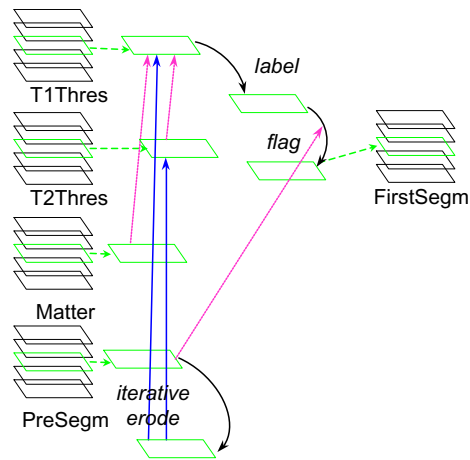


Figure 2.32: Hippocampus head and tail segmentation algorithm, traversing volume.

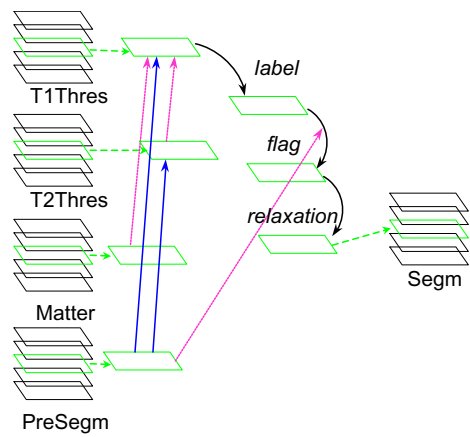


Figure 2.33: Hippocampus segmentation algorithm.

CHAPTER 3

Visualisation Techniques

There are two different ways of displaying 3D data on a 2D screen: surface rendering and volume rendering. In surface rendering, the 3D data has been modelled in some way, with only the surface of an object being stored. There is no information about inner structures of the object. Many of the most popular computer games use models like these. Computer-animated films like *Toy Story* or *Dinosaurs* from Disney's Studios use surface models. In volume rendering, the data to be displayed is true 3D; all voxels within the volume can be taken into account when viewing the volume.

Most surface rendering methods generates 2D images using a technique called ray-tracing, which means that all rays that end in the viewer's eyes are back-traced through the screen into the object scene. If the ray hits an object, the ray is reflected according to the material properties of that object and the rays penetrates no further into the object. Illumination contributes to the colour of the pixel of the screen. Figure 3.1 a) shows how rays are traced to the viewer, one ray in this example hitting the surface of the object.

Volume rendering uses internal information of the volume that is visualised. As in surface rendering, rays can be cast from the viewer through the display window and into the volume. The pixel value displayed on the screen depends on the properties of all voxels that the ray intersects. When all rays are cast, the image is complete. There are several different ways that the displayed value can be affected by the voxels the ray intersects. The pixel value may be an average of values along the ray (equivalent to a standard x-ray image), or the maximum value. Light conditions of the scene and material properties may also contribute to the displayed intensity and colour. Figure 3.1 b) illustrates the principles of ray-casting of a volume.

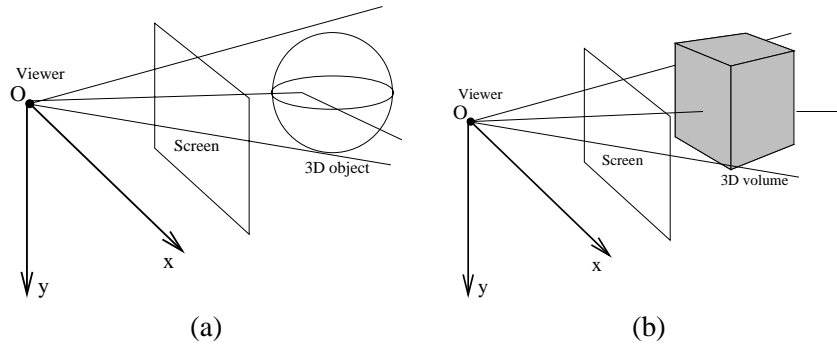


Figure 3.1: The principle behind surface rendering and volume rendering. a) Surface rendering. b) Volume rendering.

3.1 Visualisation of Thin Structures

In Paper I we describe an algorithm that generates geometric data from voxels. Triangles describing the surface are the output. Before volume rendering was implemented in the CBA program we were planning to use the algorithm for activation studies and to mix volumes from different modalities in the atlas. It is possible to visualise segmented parts together with model structures from the atlas. We needed a program that could produce a geometric model from a binary data set. The program should be easy to use and produce a result which is easy to interpret. An algorithm that is especially useful for visualising thin structures in 3D volume images is presented. Typical objects that consist of very thin structures are those generated through skeletonisation, see Figure 3.2.

A surface representation has been built, as it is quite difficult to visualise thin structures using ray-casting as a rendering method: many of the finer details will be lost. Sometimes a display of the voxels *as is*, that is, not using interpolation of any kind, is needed. If the small structures are converted into a geometric model the loss of finer details can be avoided. However, smooth shading is used as it gives a better three-dimensional impression of the scene. The algorithm scans a volume and creates a list of triangles that have a normal defined at each vertex. The visualisation is done with OpenGL rendering of geometric objects.

Several algorithms that do this already exist, the two most popular being an algorithm proposed by Lorensen and Cline, Marching Cubes [62], and one proposed by Gordon and Udupa [34]. Marching Cubes produces a vast amount of triangles in order to achieve surfaces that are smooth. As a result, this approach is very slow when displaying larger structures without polygon reduction. Gordon's and Udupa's algorithm tracks a closed surface from a set of connected cubes based on the traversal of graphs to track a 6-connected object at a time. This method is more complex than Marching Cubes. Our algorithm combines elements from both these algorithms. The output is similar to Gordon's and

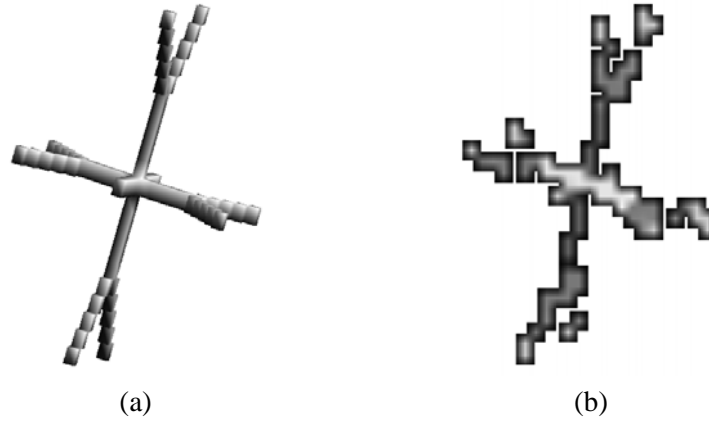


Figure 3.2: The difference between surface rendering and volume rendering of thin structures. a) Here the fine structures are shown when surface rendering is used. b) Volume rendering used to visualise a skeleton of a cross shows that some voxels are missing.

Udupa's but employs the approach from Marching Cubes in the sense that the whole volume is only traversed once and lookup tables are used to compare which neighbours a voxel has. Then the normal vectors are selected from the list. Gordon's and Udupa's approach also labels the volume but that was of no importance for our purposes and caused overhead that only slowed down the process of building the geometric model.

3.2 Visualisation of Functional Information

3.2.1 Normal material for viewing Functional Information

When analysing images of a patient, one relevant question is whether or not the image is normal or abnormal. Even an image that appears not to be completely normal might be within the normal variation when a larger sample is evaluated. When doing this kinds of analysis it can be of great help to create a normal material, ideally from a very large data set of images, that shows the normal variation of different image features. This has been done in Paper II where a normal material from a control group was created in the following way.

All scans must first be registered together and reformatted into a common anatomy, in this case the anatomy of the brain atlas described earlier. The scans must also be normalised using a normalisation method suitable for this purpose. The standard deviation and mean of the images are calculated from the control group. Then, selected ROIs from the atlas are calculated for all scans in the group. For every single ROI the mean and standard deviation are calculated for all individual voxels. Different materials can then be assembled

for variation in age or sex and for different radio-pharmaceutical substances. These different sets can then be used for patient examinations.

When performing a patient examination it is also necessary to register the scan to the brain atlas and the normalisation method used when the normal material was constructed. The same ROIs used for the normal material are also calculated for the patient data. To get a comparison, all differences in corresponding voxels from the normal material and the patient are calculated. This gives a resulting image in which it can be seen where the activity is increased or decreased compared to the normal material. Using the standard deviation image of the normal material, a Z-score image can be created, as described in Paper II. This Z-score image visualises statistical significance values for each voxel in the images. This is also done for each of the included ROIs, this giving a Z-score value for each ROI and a difference value for each ROI, which expresses of the difference and how significant the difference is for each of the ROIs, compared to the mean ROIs from the normal material. This is a way of automatising the identification of areas in SPECT scans in which the perfusion is changed.

3.2.2 3D Visualisation of Functional Information

When the images have been pre-processed using the segmentation tool, we can use the visualisation module in the CBA program to display the segmented brain. Besides displaying the segmented brain itself, it is also possible to map functional information from other examinations of the same patient using a technique called activity projection grey level gradient shading (APG). In [104] the tool for visualisation, APG, and some other visualisation techniques are described in more detail. The applications of this rendering module using a segmented cortex are described in Paper IV. In Figure 3.3 a fMRI has been mapped on a segmented MRI. All colours are pseudo-colours, which means that the actual data is grey-level but for interpretation reasons the grey level values has been mapped on a colour scale. In this case the anatomical data was registered to the functional data, that is, the resolution was reduced to slice dimensions 79×95 with 68 slices.

The anatomical information on which to map the functional data may be the patient's own anatomy of the brain from a T1-MRI segmented cortex using the method described in Paper III, Paper V or Paper VI. If no anatomical data exist it is possible to binarise the atlas version of the brain surface and use this to map the functional data. The functional data must be registered with the brain atlas and, if present, with the anatomical data set.

The fusion of functional and anatomical data that are visualised in 3D can be a comprehensive and valuable presentation technique with a significant diagnostic value for the physicians.

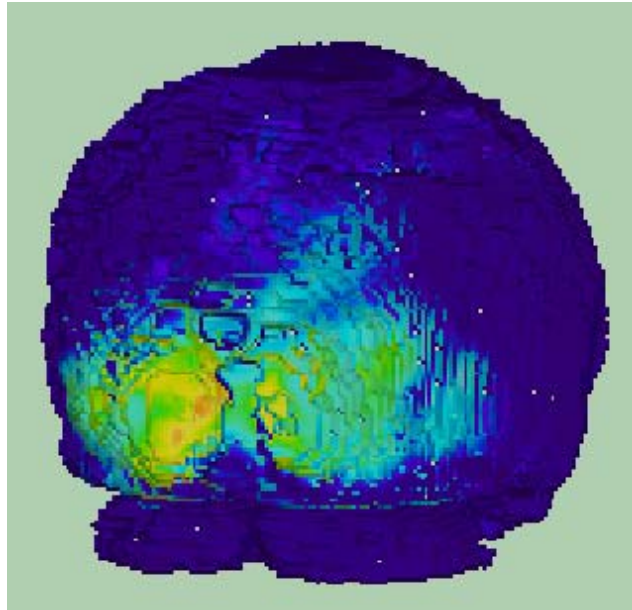


Figure 3.3: Activated regions of a fMRI mapped onto a segmented MRI which has been visualised using volume rendering. See page 66 for a colour version of the figure.

Here follows a brief description of how the visualisation of functional data on a segmented brain works. Rays are cast into the segmented volume and when the border is reached, a calculation of the normal in that point is performed. Then a new ray is cast in the functional volume, with a direction that is opposite to that of the normal vector. The ray travels a certain distance into the functional volume. The desired distance depends on how the volume was acquired and can be set by the user. All intensity levels are checked along the ray, and the maximum activity value along that line is then selected to change the display colour for the intersection between the first ray and the segmented volume. Not only a colour is determined, but also other material parameters. Shading is used to increase the perception that the image is a 3D projected on a 2D surface. The Phong illumination model is used. [82].

There is one other method that works in a way similar to the method used in the CBA program. That method is called *Normal Fusion* and was proposed by Stokking et al [95]. The main differences concern how functional data are combined with anatomical data. The name *Normal Fusion* refers to its projecting regional information sampled along the inward normal of a surface onto the surface. The method also uses the Phong illumination model.

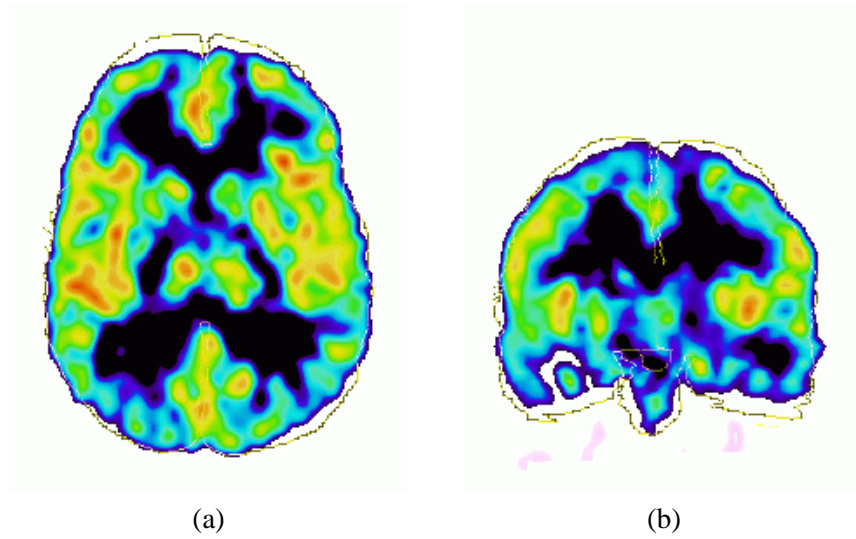


Figure 3.4: An activation of the brain. A transaxial slice (left) and a coronal slice (right) with the contours of the brain atlas that are used as an anatomical reference. See page 66 for a colour version of the figure.

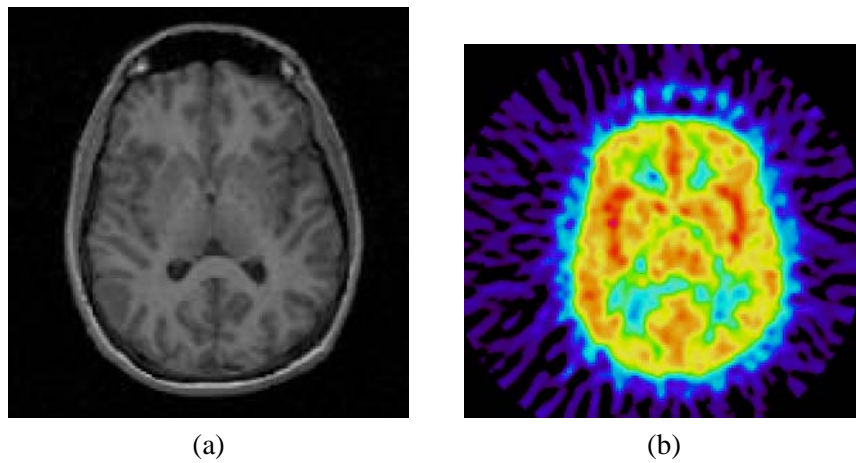


Figure 3.5: The original a) MRI and b) PET volumes. See page 66 for a colour version of the figure.

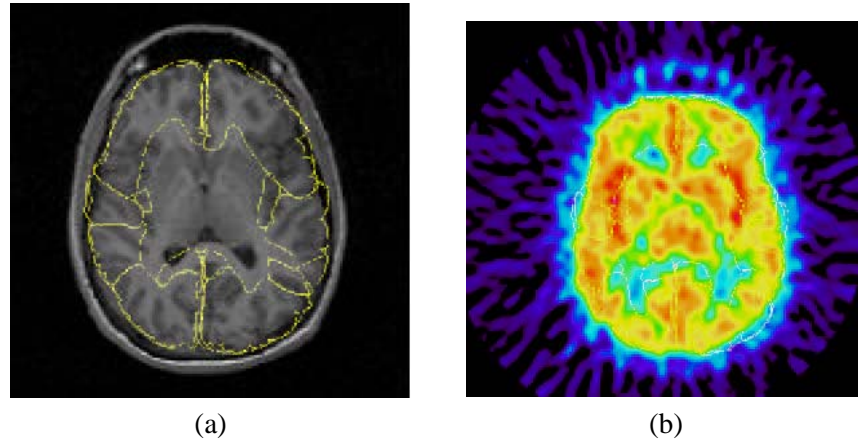


Figure 3.6: The a) MRI and b) PET volumes with structures from the computerised brain atlas. See page 67 for a colour version of the figure.

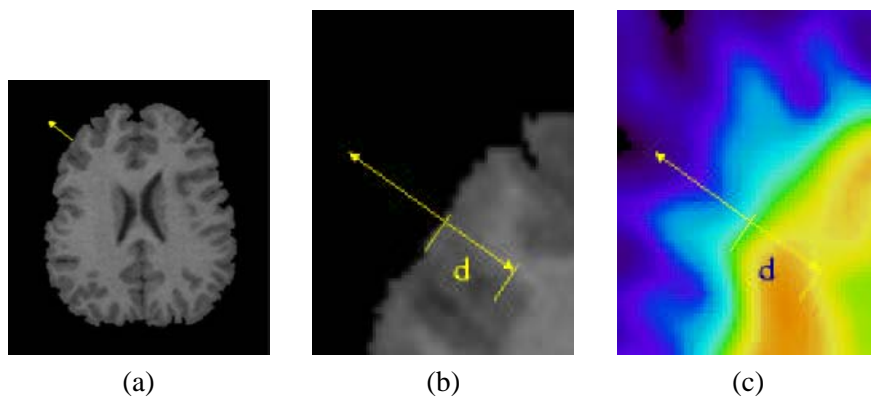


Figure 3.7: a) Segmented MRI with b) normal and c) PET with the same normal and depth to be checked. See page 67 for a colour version of the figure.

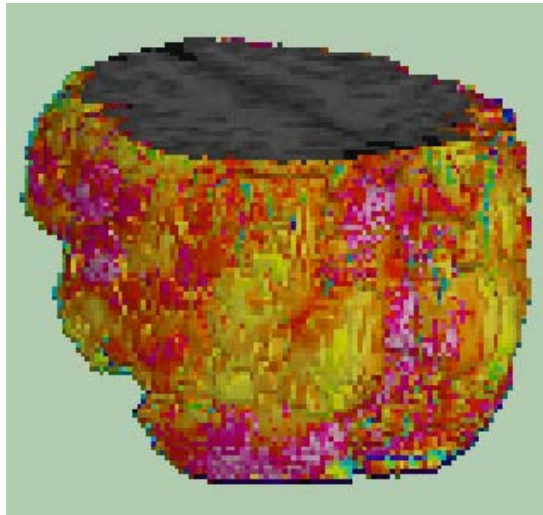


Figure 3.8: The same data as in Figure 3.4. The APG method was used to map the activated areas onto the surface of segmented MRI of the same patient. See page 68 for a colour version of the figure.

CHAPTER 4

Autoradiography

The imaging modalities described so far have the advantage that they can image the brains of living persons. But they have limited resolution, 0,5 mm at best.

In Paper VIII, post-mortem analysis of autoradiographic images has been investigated. Autoradiography using human postmortem brain whole hemisphere cryosections provides high image resolution (about 50 μm) and is therefore suitable for the detailed anatomical description of neuroreceptor distributions [22], [37], [90]. This methodology has frequently been applied for the examination of the distribution and quantification of receptor subtypes of several neurotransmitter systems in the brain. One limitation to this methodology is that the image analysis procedure that has been used prior to this work can be very time-consuming. The normal procedure after digitisation is that several ROIs are drawn manually on the autoradiograms in the sequence. Drawing the same ROI on different sections also increases the possibility of errors in the measurements. The image analysis method in Paper VIII reduces the need for manual drawing.

The images were first compensated for background shading. The sections in each study were registered together using the anatomical reference image (Cresyl violet-stained or Nissl stained). This was done to minimise the risk of drifting or gradual rotation. What may happen otherwise can be seen in Figure 4.1.

The serotonin transporters were visualised using [^3H]citalopram. Radiosynthesis of the 5-HT_{1A} receptor antagonist [^3H]WAY-100635 was performed using O-desmethyl-WAY-100635 and [^3H]methyl iodide. For the labelling of 5-HT_{1B} receptors, [^3H]GR 125743 was employed. The 5-HT_{2A} antagonist [^3H]M100907 was prepared from the 3-hydroxy precursor (MDL 105725) using [^3H]methyl iodide.

The three brains in this study were cryosectioned with a thickness of 100 μm and transferred to gelatinised or poly-L-lysine-treated glass plates. To get an anatomical reference, a section at each level were stained with cresyl violet

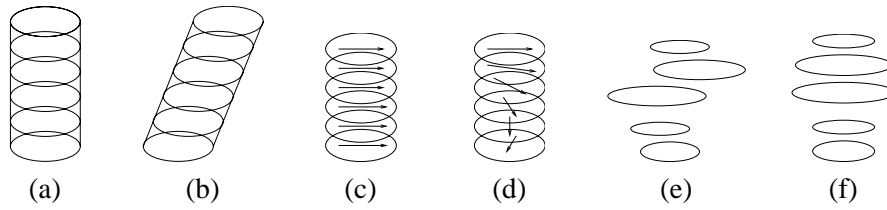


Figure 4.1: Alignment of serial sections with translation through an inclined circular cylinder a), may be misconstrued and start to drift towards one of the sides b). Alignment of serial sections may cause a false rotation in the output, where c) is the actual outlines in correct 3D serial section stack and d) is the erroneous result. Alignment of serial sections with translation may also be lost in the output, where e) is the correct 3D serial section stack and f) is the erroneous result.

(Nissl staining). Autoradiographic films were applied to the sections for 10–13 weeks and were digitised using a flat-bed scanner.

Due to imperfections in the image acquisition the background is compensated for, see Figure 4.2. The method is described in greater detail elsewhere [61]. Cubic B-splines are being used to describe the bias field. The cubic B-splines are useful because they are always smooth and can be easily controlled. When the bias field is estimated it is removed from the original image.

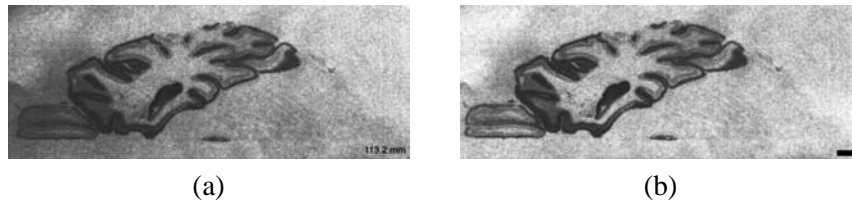


Figure 4.2: Background compensation of an autoradiogram showing total [^3H]WAY-100635 binding. (a) Original image obtained by digitisation using a flatbed scanner. To enhance the shading effect the image has been normalised and mean filtered. (b) Image obtained after background compensation. This image has also been normalised and mean filtered to show that most of the shading has been removed.

After background compensation the images are registered using mutual information matching [108], [16], [64], [96], [97], [84] on detailed images; hierarchical chamfer matching [10], [69] on images with less detail, but with some

strong contours; and manual matching on images containing too little information for automatic matching.

The images were transformed into binding densities (pmol/g tissue equivalents) using log-log linear calibration functions ($y=c_1 10^{(\log(255-x))} + c_2$), with the use of autoradiographic ^3H -calibrating scales. To obtain images representing the specific binding densities, the non-specific binding was subtracted from the total binding (Fig. 4.3).

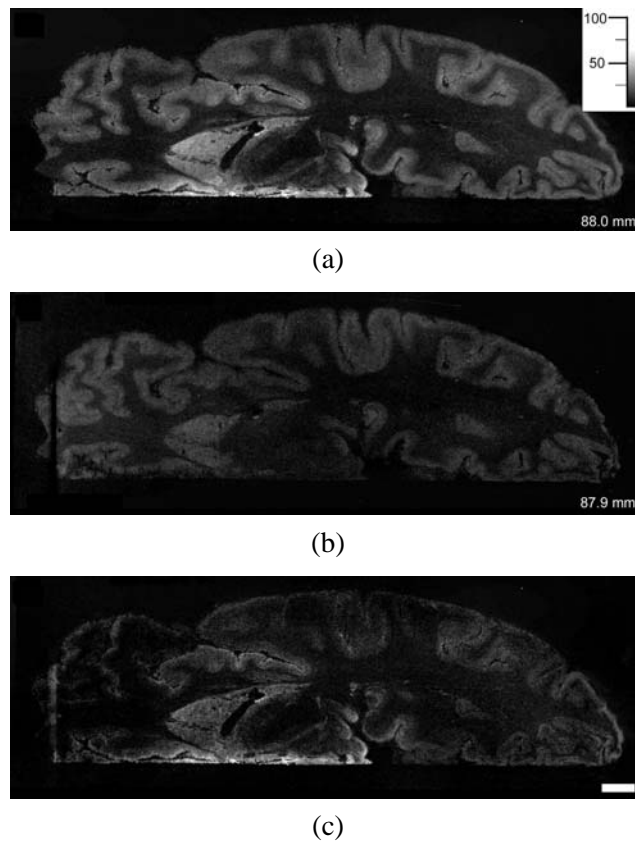


Figure 4.3: Visualisation of the specific binding densities of [^3H]citalopram. The specific binding to the 5-HT transporter was obtained by subtraction of the non-specific binding from the total binding. (a) Total [^3H]citalopram binding. (b) Non-specific binding of [^3H]citalopram in the presence of 10 μM fluoxetine. (c) Specific binding of [^3H]citalopram to the 5-HT transporter. Values are expressed in pmol/g tissue, original wet weight. The vertical line in (b) and (c) is due to a tear in the emulsion. Numbers in the lower right corner represent distance (in mm) from the vertex.

The different structures were semi-automatically segmented using the same

KDE method as before [60], [87], [80]. ROIs can be selected in the section where they are easiest to delineate, see Figure 4.4 a and using the nissl image for anatomical reference, see Figure 4.4 b-c). This corrected ROI can be used for measurements, see Figure 4.5).

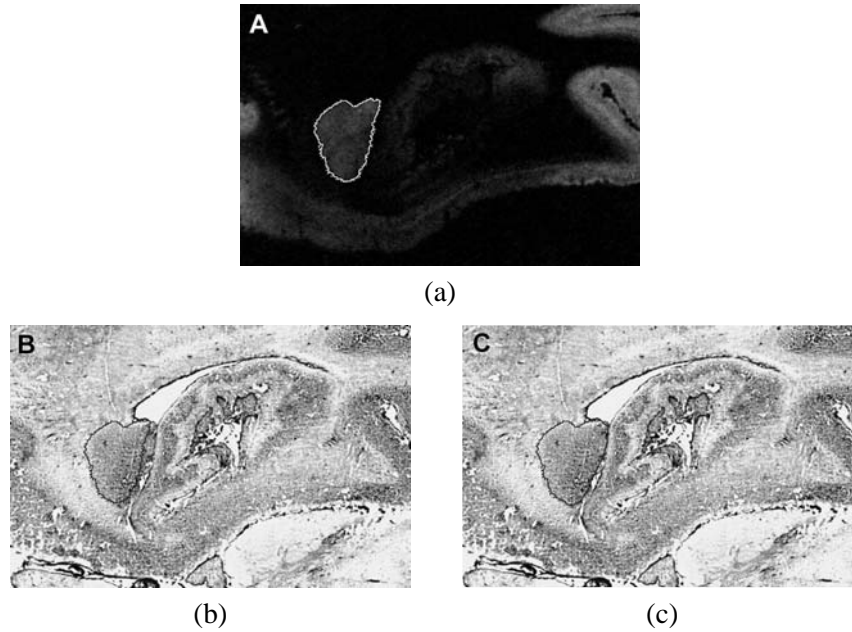


Figure 4.4: Regions of interest (ROI) definition by computerised image analysis, see methods for detailed description. (a) 5-HT_{2A} receptor binding with initially segmented ROI of the basolateral amygdala. (b) Cresyl violet stain with ROI transferred from A. (c) Cresyl violet stain with edited ROI.

A standard method for working with autoradiographic images is the use of a phosphor imager and image processing and analysis, performed by Science Lab 98, L Process 1.72 and Image Gauge 3.12. The ROIs are delineated manually on each image. The binding densities obtained using this method are in most cases in good agreement with the densities found using the new method. The problems encountered might be due to saturation of the film in high intensities or because of the lower spatial resolution of the phosphor imager, 100 vs. 50 μm .

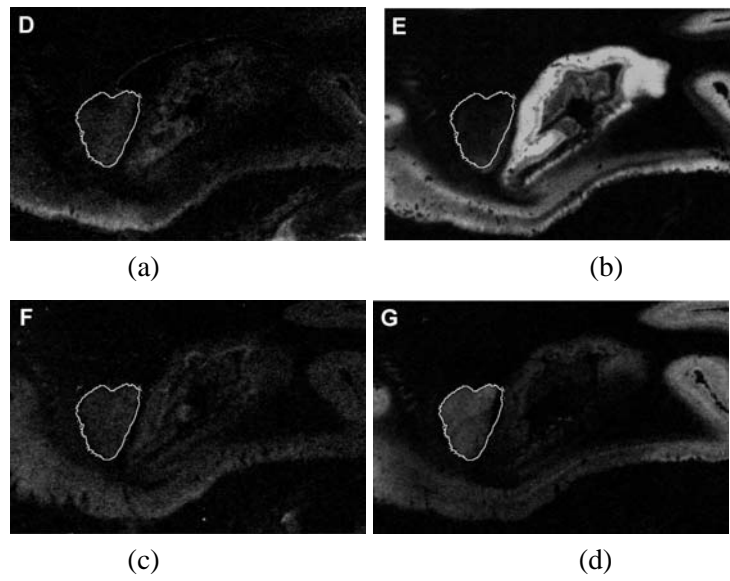


Figure 4.5: Images representing specific binding with superimposed ROI for $[^3\text{H}]$ citalopram (a), $[^3\text{H}]$ WAY-100635 (b), $[^3\text{H}]$ GR125743 (c) and $[^3\text{H}]$ M100907 (d). In (b), further editing of the ROI may be required. For visualisation purposes, a) and c) were multiplied by 2.

CHAPTER 5

Conclusion

In this thesis it has been shown that segmentation of the cortex can be used to produce integrated presentations of functional and anatomical brain images. The visualised 3D volume provides a powerful tool for finding significant information that is harder to retrieve when viewing 2D slices. The segmentation of the hippocampus improves an existing method significantly. The image processing and image analysis of autoradiographic images described in this thesis improves the speed and accuracy compared to standard methods.

5.1 Discussion

When working with a substantial amount of data it is desirable to avoid user-interaction as much as possible since it soon becomes too time-consuming. We have successfully replaced manual segmentation with an automatic algorithm. The cortex segmentation algorithm has been visually evaluated on 30 patient data sets with a mix of transaxial, sagittal, and coronal cases. Problems that we have encountered include strong connections between the cortex and surrounding tissue if the data was resampled to a much lower resolution or the intensity resolution was very poor. The first case with low spatial resolution occurred when an MRI was registered to fit a functional data set, see Figure 5.1. Further problems are that the algorithm does not handle severely shaded volumes very well. The main reason for this is our use of the mid-slice only as a base for the automatic thresholding.

The hippocampus segmentation algorithm has been evaluated with the use of 30 manually segmented patient data sets. The segmentation was done by an experienced scientist. The original ANN based method only finds about 60% of the volumes when compared to the hand traced volumes, but the combined method finds at least 90% of the volume. The manual tracer often includes areas not visible in the images, as a smoother shape seems to be more desirable. When using the original method, corrections on as many as half of the slices

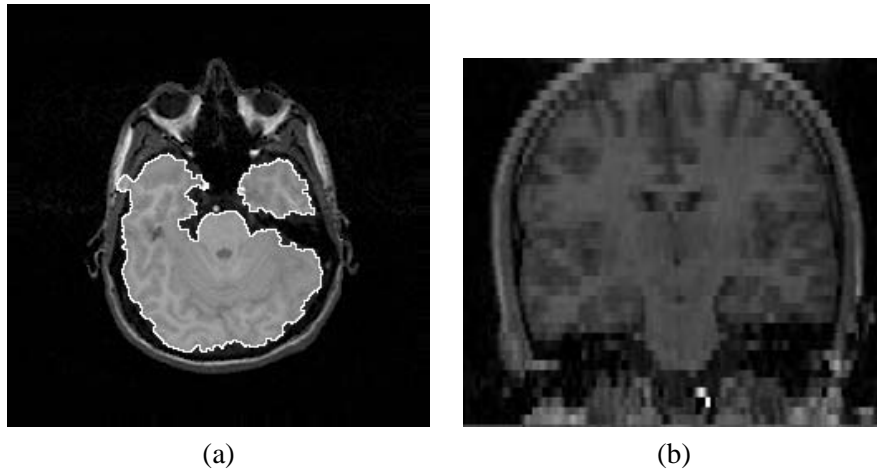


Figure 5.1: Troublesome volume due to down sampling. a) A slice where the algorithm failed due to the neighbourhood information being insufficient in the down-sampled volume. b) A coronal view of the volume. It is clearly visible that the thickness of the slices is large.

was necessary, but when using the combined method only a few slices have to be manually corrected.

Visualisation of 3D data is also important. Visualisation can be a tool to interpret what is present in a set of functional and anatomic images, which means that important areas should be clearly visible. The computerised brain atlas is capable of registration and segmentation as well as visualisation of the image data. The visualisation may be done either as a 3D ray-casted image with combined functional and anatomical information, or as the functional data converted to a geometric model and displayed together with a geometric model of brain structures.

Thin structures such as produced by skeleton algorithms [11] are not easy to visualise using volume rendering. It is sometimes necessary to convert the voxels to geometric data and use surface rendering to display the skeleton.

In this thesis, image analysis methods have also been applied to images of autoradiographic origin. These new methods are a definite improvement on earlier ones. Earlier, when measurements were performed, the same ROI had to be drawn on each of the sections to be analysed. It was also not possible to create an image with specific bindings. The solution to these two problems was registration. Furthermore, the scanned plates were shaded and this was also successfully accounted for.

5.2 Future Work and Improvements

The tool for cortex segmentation now handles all three acquiring directions of T1-weighted MRIs, that is transaxial, sagittal and coronal acquisition protocols. When the T1-weighted MRIs are resampled to isotropic voxels and if anisotropic data any of the methods should work. The three algorithms can be used in sequence and the result combined, as is the case with the hippocampus segmentation.

It would be interesting to investigate methods that standardise a MRI intensity scale [76], [77]. This should reduce problems when classifying the tissue types in the MRI data.

The problem that always arises in MRI images is background shading due to inhomogeneities in the coil of the MR camera. Several methods to compensate for the shading effect exist [13].

The thresholds found on adjacent slices might vary due to variations in the amount of different tissue types in the image, an extreme example of this is the central sagittal slice between the two brain halves. The problem with changed thresholds appears on other slices as well, in all three directions. To cope with this problem, it should be possible to place a constraint in the histogram thresholding that ensures that the threshold values do not differ too much between adjacent slices. This problem has so far been addressed by using only a few slices when searching for threshold values, i.e. the starting slices have been used.

Further development of segmentation algorithms and other applications will be carried out in close collaboration with the Human Brain Informatics (HUBIN) group at Karolinska Hospital [3]. The new methods may combine grey-level morphology and artificial neural nets (ANN). A large data base of coronal MRI scans is thus available to the HUBIN group.

The drawing of new atlas structures for the new atlas, based on the average of co-registered MRIs, requires a new improved Windows 9x/NT based drawing program. This also requires a new and integrated triangulation algorithm that could be used for segmented images as well, combined with a method to reduce the number of polygons produced.

Improvement of the surface rendering module in CBA to make it possible to use a texture map of functional data on geometric models (either from atlas structures or generated from segmented data) is also desirable. This would yield a faster display when using real time interaction.

References

- [1] J. L. R. Andersson. A Rapid and Accurate Method to Realign PET Scans Utilizing Image Edge Information. *Journal of Nuclear Medicine*, 36:657–669, 1995.
- [2] J. L. R. Andersson and L. Thurfjell. Implementation and Validation of a Fully Automatic System for Intra- and Inter-Individual Registration of PET Brain Scans. *Journal of Computer Assisted Tomography*, 21(1):136–144, 1997.
- [3] S. Arnborg, I. Agartz, M. Nordström, H. Hall, and G. Sedvall. Human Brain Informatics - Understanding Causes of Mental Illness. *ERCIM News*, (43), October 2000.
- [4] M. S. Atkins and M. T. Mackiewicz. Fully Automatic Segmentation of the Brain in MRI. *IEEE Transactions on Medical Imaging*, 17(1):98–107, February 1998.
- [5] P. Bartenstein, S. Minoshima, C. Hirsch, K. Buch, F. Willoch, D. Mösch, D. Schad, M. Schwaiger, and A. Kurz. Quantitative Assessment of Cerebral Blood Flow in Patients with Alzheimer’s Disease by SPECT. *Journal of Nuclear Medicine*, 38:1095–1101, 1997.
- [6] J. Beutel, H. L. Kundel, and R. L. Van Metter, editors. *Medical Imaging Volume 1. Physics and Psychophysics*, chapter 6, pages 375–461. SPIE Press, 2000.
- [7] C. Bohm, T. Greitz, and B. M. Berggren. Selection of PET ROIs from a Computerized Brain Atlas. *Journal of Cerebral Blood Flow Metabolism*, 5:S613–S614, 1985. Suppl1.
- [8] C. Bohm, T. Greitz, D. Kingsley, B. M. Berggren, and L. Olsson. Adjustable Computerized Stereotaxic Brain Atlas for Transmission and Emission Tomography. *American Journal of Neuroradiology*, 4:731–733, 1983.

- [9] C. Bohm, T. Greitz, R. Seitz, and L. Eriksson. Specification and Selection of Regions of Interest (ROIs) in a Computerized Brain Atlas. *Journal of Cerebral Blood Flow Metabolism*, 11:A64–A6, 1991.
- [10] G. Borgefors. On Hierarchical Edge Matching In Digital Images Using Distance Transforms. Technical report, NADA, KTH, Sweden, 1986. TRITA-NA-8602.
- [11] G. Borgefors, I. Nyström, and G. Sanniti di Baja. Surface Skeletonization of Volume Objects. In P. Perner, P. Wang, and A. Rosenfeld, editors, *Advances in Structural and Syntactical Pattern Recognition*, 6th International Workshop, SSPR '96 Leipzig, Germany, August 1996, pages 251–259. Structural and Syntactical Pattern Recognition, Springer-Verlag Berlin Heidelberg, August 1996.
- [12] M. E. Brummer, R. M. Mersereau, R. L. Eisner, and R. R. J. Lewine. Automatic Detection of Brain Contours in MRI Data Sets. *IEEE Transactions on Medical Imaging*, 12(2):153–166, June 1993.
- [13] G. G. C. Brechbühler and G. Székely. Compensation of Spatial Inhomogeneity in MRI Based on a Parametric Bias Estimate. In *Proceedings of the Fourth International Conference on Visualization in Biomedical Computing (VBC'96)*, pages 141–146, Hamburg, Germany, September 1996. Springer.
- [14] I. Carlbom, G. Klinker, D. Terzopoulos, and L. Thurfjell. General-Purpose Soft Tissue Segmentation from Medical Images. In *Proceedings of 9th Scandinavian Conference on Image Analysis, Uppsala, Sweden*, pages 905–912, 1995.
- [15] L. R. Clarke, R. P. Velthuisen, M. A. Camacho, J. J. Heine, M. Vaidyanathan, L. O. Hall, R. W. Thatcher, and M. Silbiger. MRI Segmentation: Methods and Applications. *Magnetic Resonance Imaging*, 13(3):343–368, 1995.
- [16] A. Collignon, F. Maes, D. Delaere, D. Vandermeulen, P. Suetens, and G. Marchal. Automated Multi-Modality Image Registration based on Information Theory. In *Proc. of Information Processing in Medical Imaging*, pages 263–274, Ile de Berder, France, 1995.
- [17] T. F. Cootes and C. J. Taylor. Active Shape Models. Draft from a forthcoming report on ASM, 1998.
- [18] T. F. Cootes, C. J. Taylor, D. H. Cooper, and J. Graham. Active Shape Models — Their Training and Application. *Computer Vision and Image Understanding*, 61(1):38–59, January 1995.

- [19] W. R. Crum, R. I. Scahill, and N. C. Fox. Automated Hippocampal Segmentation by Regional Fluid Registration of Serial MRI: Validation and Application in Alzheimer's Disease. *NeuroImage*, 13(5):847–855, May 2001.
- [20] J. Declerck, G. Subsol, J. Thirion, and N. Ayache. Automatic Retrieval of Anatomical Structures in 3D Medical Images. In N. Ayache, editor, *Information Processing, Virtual Reality and Robotics in Medicine*, volume 905 of *Lecture Notes in Computer Science*. Springer-Verlag, 1995.
- [21] A. Evans, C. Beil, S. Marett, C. Thompson, and A. Hakim. Anatomical-functional Correlation Using an Adjustable MRIbased Region of Interest Atlas with Positron Emission Tomography. *Journal of Cerebral Blood Flow Metabolism*, 9:513–530, 1988.
- [22] L. Farde and H. Hall. Positron Emission Tomography-Examination of Chemical Transmission in the Living Human Brain. Development of Radioligands. *Arzneimittel-Forschung*, 42(2A):260–264, 1992.
- [23] B. Fischl, D. H. Salat, E. Busa, M. Albert, M. D. C. Haselgrove, A. van der Kouwe, R. Killiany, D. Kennedy, S. Klaveness, A. Montillo, N. Makris, B. Rosen, and A. M. Dale. Whole Brain Segmentation: Automated Labeling of Neuroanatomical Structures in the Human Brain. *Neurotechnique*, 33(3):341–355, January 2002.
- [24] P. Fox and M. Raichle. Enhanced Detection of Focal Brain Responses Using Intersubject Averaging and Change-Distribution Analysis of Subtracted PET Images. *Journal of Cerebral Blood Flow Metabolism*, 8:642–653, 1988.
- [25] P. T. Fox, J. S. Perlmuter, and M. E. Raichle. A Stereotactic Method of Anatomical Localization for Positron Emission Tomography. *Journal of Computer Assisted Tomography*, 9(1):141–153, 1985.
- [26] K. J. Friston, C. D. Frith, P. F. Liddle, and R. S. J. Frackowiak. Comparing Functional (PET) Images: the Assessment of Significant Change. *Journal of Cerebral Blood Flow Metabolism*, 11:690–699, 1991.
- [27] K. J. Friston, R. E. Passingham, J. G. Nutt, J. D. Heather, G. V. Sawle, and R. S. J. Frackowiak. Localisation in PET Images: Direct Fitting of the Intercommissural (AC-PC) Line. *Journal of Cerebral Blood Flow Metabolism*, 9:690–695, 1989.
- [28] K. J. Friston, K. J. Worsley, R. S. J. Frackowiak, J. C. Mazziotta, and A. C. Evans. Assessing the Significance of Focal Activations Using Their Spatial Extent. *Human Brain Mapping*, 1:210–220, 1994.

- [29] M. Garza-Jinich, P. Meer, and V. Medina. Robust Retrieval of 3D Structures from Magnetic Resonance Images. In *Proceedings of the 13th International Conference on Pattern Recognition*, volume III, pages 391–395, Vienna, Austria, August 1996. IAPR, IEEE Computer Society Press, Los Alamitos, California.
- [30] J. Gee, M. Reivich, and R. Bajscy. Elastically Deforming 3D Atlas to Match Anatomical Brain Images. *Journal of Computer Assisted Tomography*, 17(2):225–236, 1993.
- [31] R. C. Gonzalez and R. E. Woods. *Digital Image Processing*, chapter 8, pages 518–560. Addison-Wesley Publishing Company, Inc., 3 edition, 1992.
- [32] R. C. Gonzalez and R. E. Woods. *Digital Image Processing*, chapter 8, pages 519–560. Addison-Wesley Publishing Company, Inc., 2 edition, 2002.
- [33] R. C. Gonzalez and R. E. Woods. *Digital Image Processing*, chapter 8, pages 550–560. Addison-Wesley Publishing Company, Inc., 2 edition, 2002.
- [34] D. Gordon and J. K. Udupa. Fast Surface Tracking in Three-Dimensional Binary Images. *Computer Vision, Graphics, and Image Processing*, 45:196–214, 1989.
- [35] T. Greitz, C. Bohm, S. Holte, and L. Eriksson. A Computerized Brain Atlas: Construction Anatomical Content, and Some Applications. *Journal of Computer Assisted Tomography*, 15(1):26–38, 1991.
- [36] T. Greitz, S. Holte, C. Bohm, L. Eriksson, R. Seitz, E. K., H. Nybäck, and S. Stone-Elander. A Data Base Library as a Diagnostic Aid in Neuroimaging. *Neuroradiology*, 33 (suppl):2–4, 1991.
- [37] H. Hall, L. Farde, C. Halldin, Y. L. Hurd, S. Pauli, and G. Sedvall. Autoradiographic Localization of Extrastriatal D₂-Dopamine Receptors in the Human Brain Using [¹²⁵I]Epidepride. *Synapse*, 23(2):115–123, 1996.
- [38] H. Hall, L. Farde, C. Halldin, C. Lundkvist, and G. Sedvall. Autoradiographic Localization of 5-HT_{2A} Receptors in the Human Brain Using [3H]M100907 and [¹¹C]M100907. *Synapse*, 38(4):421–431, 2000.
- [39] H. Hall, C. Halldin, L. Farde, and G. Sedvall. Whole Hemisphere Autoradiography of the Postmortem Human Brain. *Nuclear Medicine & Biology*, 25(8):715–719, 1998.

- [40] H. Hall, C. Halldin, D. Guilloteau, S. Chalon, P. Emond, J. Besnard, L. Farde, and G. Sedvall. Visualization of the Dopamine Transporter in the Human Brain Postmortem With the New Selective Ligand [125 I]PE $_2$. *NeuroImage*, 9(1):108–116, 1999.
- [41] H. Hall, Y. Hurd, S. Pauli, C. Halldin, and G. Sedvall. Human Brain Imaging Post-Mortem - Whole Hemisphere Technologies. *International Review of Psychiatry*, 13:12–17, 2001.
- [42] H. Hall, J.-E. Litton, C. Halldin, J. Kopp, and G. Sedvall. Studies on the Binding of [3 H]Flumazenil and [3 H]Sarmazenil in Post-Mortem Human Brain. *Human Psychopharmacology*, 7:367–377, 1992.
- [43] H. Hall, C. Lundkvist, C. Halldin, L. Farde, V. W. Pike, J. A. McCarron, A. Fletcher, I. A. Cliffe, T. Barf, H. Wikström, and G. Sedvall. Autoradiographic Localization of 5-HT $_{1A}$ Receptors in the Post-Mortem Human Brain Using [3 H]WAY-100635 and [11 C]WAY-100635. *Brain Research*, 745(1–2):96–108, 1997.
- [44] K. Hall, G. Sedvall, O. Magnusson, J. Kopp, C. Halldin, and L. L. Farde. Distribution of D $_1$ - and D $_2$ -Dopamine Receptors, and Dopamine and its Metabolites in the Human Brain. *Neuropsychopharmacology*, 11(4):245–256, 1994.
- [45] J. W. Haller, A. Bannerjee, G. E. Christensen, M. Gado, S. Joshi, M. Miller, M. I. Sheline, M. W. Vannier, and J. G. Csernansky. Three-Dimensional Hippocampal MR Morphometry with High-Dimensional Transformation of a Neuroanatomic Atlas. *Radiology*, 51(4):993–999, 1997.
- [46] G. Harris, N. C. Andreasen, T. Cizadlo, J. M. Bailey, H. J. Bockholt, V. A. Magnotta, and S. Arndt. Improving Tissue Classification in MRI: A Three-Dimensional Multispectral Discriminant Analysis Method with Automated Training Class Selection. *Journal of Computer Assisted Tomography*, 23(1):144–154, January 1999.
- [47] T. Heinonen, H. Eskola, P. Dastidar, P. Laarne, and J. Malmivuo. Segmentation of T1 MR Scans for Reconstruction of Resistive Head Models. *Computer Methods and Programs in Biomedicine*, 54(3):173–181, November 1997.
- [48] K. H. Höhne and W. H. Hanson. Interactive 3D Segmentation of MRI and CT Volumes Using Morphological Operations. *Journal of Computer Assisted Tomography*, 16(2):285–294, 1992.

- [49] R. Hult. Grey-level Morphology Based Segmentation of MRI of the Human Cortex. In *Proceedings of ICIAP01 11th International Conference on Image Analysis and Processing, Palermo, Italy*, pages 578–583, September 2001.
- [50] R. Hult. Segmentation of T1-MRI of the Human Cortex Using a 3D Grey-level Morphology Approach. In J. Bigun and T. Gustavsson, editors, *Image Analysis, 13th Scandinavian Conference, SCIA 2003, Halmstad, Sweden, Proceedings*, volume 2749 of *LNCS*, pages 462–469. Springer, June/July 2003.
- [51] R. Hult and E. Bengtsson. Combined Visualisation of Functional and Anatomical Brain Images. In *Proceedings of 12th Scandinavian Conference on Image Analysis, Bergen, Norway*, volume I, pages 84–89, 2001.
- [52] R. Hult, E. Bengtsson, and L. Thurffjell. Surface Construction Especially Suited for Visualisation of Thin Structures. In *Proceedings of 10th Scandinavian Conference on Image Analysis, Lappeenranta, Finland*, volume I, pages 359–363, 1997.
- [53] R. Hult, E. Bengtsson, and L. Thurffjell. Segmentation of the Brain in MRI Using Grey Level Morphology and Propagation of Information. In *Proceedings of 11th Scandinavian Conference on Image Analysis, Kangerlussuaq, Greenland*, volume I, pages 367–373, 1999.
- [54] M. Ingvar, L. Eriksson, T. Greitz, S. Stone-Elander, M. Dahlbom, G. Rosenqvist, P. af Trampe, and C. von Euler. Methodological Aspects of Brain Activation Studies: Cerebral Blood Flow Determined with [15O]butanol and Positron Emission Tomography. *Journal of Cerebral Blood Flow Metabolism*, 14:628–638, 1994.
- [55] A. Kak and M. Slaney. *Principles of Computerized Tomographic Imaging*. IEEE Press, 1987.
- [56] A. Kelemen, G. Szekely, and G. Gerig. Elastic Model-Based Segmentation of 3-D Neuroradiological Data Sets. *IEEE Transactions on Medical Imaging*, 18(10):828–839, October 1999.
- [57] D. H. Laidlaw, K. W. Fleischer, and A. H. Barr. Partial-Volume Bayesian Classification of Material Mixtures in MR Volume Data Using Voxel Histograms. *IEEE Transactions on Medical Imaging*, 17(1):74–86, February 1998.

- [58] T.-C. Lee, R. L. Kashyap, and C.-N. Chu. Building Skeleton Models via 3-D Medial Surface/Axis Thinning Algorithms. *CVGIP: Graphical Models and Image Processing*, 56(6):462–478, 1994.
- [59] C. Li, D. B. Goldgof, and L. O. Hall. Knowledge-Based Classification and Tissue Labeling of MR Images of Human Brain. *IEEE Transactions on Medical Imaging*, 12(4):740–750, December 1993.
- [60] J. Lindblad. Histogram Thresholding using Kernel Density Estimates. In *Proceedings of SSAB (Swedish Society for Automated Image Analysis) Symposium on Image Analysis, Halmstad, Sweden*, pages 41–44, March 2000.
- [61] J. Lindblad and E. Bengtsson. A Comparison of Methods for Estimation of Intensity Nonuniformities in 2D and 3D Microscopy Images of Fluorescence Stained Cells. In *Proceedings of 12th Scandinavian Conference on Image Analysis, Bergen, Norway*, 2001.
- [62] W. E. Lorensen and H. E. Cline. Marching Cubes: A High Resolution 3D Surface Construction Algorithm. *Computer Graphics*, 21(3):163–169, July 1987.
- [63] R. Lundqvist. *Atlas-Based Fusion of Medical Brain Images. Methods and Applications*. PhD thesis, Uppsala University, 2001.
- [64] F. Maes, A. Collignon, D. Vandermuelen, G. Marchal, and P. Suetens. Multimodality Image Registration by Maximization of Mutual Information. *IEEE Transactions on Medical Imaging*, 16(2):187–198, April 1997.
- [65] V. A. Magnotta, G. Harris, N. C. Andreasen, D. S. O’Leary, W. T. Yuh, and D. Heckel. Structural MR Image Processing using the BRAINS2 Toolbox. *Computerized Medical Imaging, Graphics*, 26:251–264, 2002.
- [66] V. A. Magnotta, D. Heckel, N. C. Andreasen, T. Cizadlo, P. W. Corson, J. C. Ehrhardt, and W. T. Yuh. Measurement of Brain Structures with Artificial Neural Networks: Two- and Three-Dimensional Applications. *Radiology*, 211(3):781–790, June 1999.
- [67] J. B. A. Maintz and M. A. Viergever. A Survey of Medical Image Registration. *Medical Image Analysis*, 2(1):1–36, 1998.
- [68] T. Mantere, E. Tupala, H. Hall, T. Sarkioja, P. Rasanen, K. Bergstrom, J. Callaway, and J. Tiuhonen. Serotonin Transporter Distribution and Density in the Cerebral Cortex of Alcoholic and Nonalcoholic Comparison Subjects: a Whole-Hemisphere Autoradiography Study. *American Journal of Psychiatry*, 159(4):599–606, 2002.

- [69] M. Melin. Implementation of the Hierarchical Chamfer Matching Algorithm on a General Purpose Image Analysis System. Technical report, Institute of technology, Uppsala University, Sweden, 1994. UPTEC 94 136E.
- [70] S. Minoshima, R. Koeppe, K. Frey, and D. Kuhl. Anatomic Standardization: Linear Scaling and Nonlinear Warping of Functional Brain Images. *Journal of Nuclear Medicine*, 35:1528–1537, 1994.
- [71] S. Minoshima, R. Koeppe, M. Mintun, K. Berger, S. Taylor, K. Frey, and D. Kuhl. Automated Detection of the Intercommissural Line for Stereotactic Localization of Functional Brain Images. *Journal of Nuclear Medicine*, 34, 322–329 1993.
- [72] J. R. Moeller and S. C. Strother. A Regional Covariance Approach to the Analysis of Functional Patterns in Positron Emission Tomographic Data. *Journal of Cerebral Blood Flow Metabolism*, 11(S1):121–135, 1991.
- [73] R. Momenan, D. Hommer, R. Rawlings, Ruttimann, M. Kerich, and D. Rio. Intensity-Adaptive Segmentation of Single-Echo T1-Weighted Magnetic Resonance Images. *Human Brain Mapping*, 5(3):194–205, 1997.
- [74] J. Nieder, T. Davis, and M. Woo. *OpenGL Programming Guide: The Official Guide to Learning OpenGL, Release 1*. Addison Wesley, 1993.
- [75] B. Nordin. IPAD, version 2.0 & IMP - an IPAD application. Internal Report 6, Centre for Image Analysis, Uppsala, Sweden, 1997. Available from the author.
- [76] L. G. Nyúl and J. K. Udupa. On Standardizing the MR Image Intensity Scale. *Magnetic Resonance in Medicine*, 42:1072–1081, 1999.
- [77] L. G. Nyúl and J. K. Udupa. Standardizing the MR Image Intensity Scales: Making MR Intensities have Tissue Specific Meaning. In *Medical Imaging 2000: Image Display and Visualization*. Proceedings of SPIE 3976, 2000.
- [78] OpenGL Architecture Review Board. *OpenGL Reference Manual: The Official Reference Document for OpenGL, Release 1*. Addison Wesley, 1992.
- [79] J. Pantel, D. S. O’Leary, K. Cretsinger, H. J. Bockholt, H. Keefe, V. A. Magnotta, and N. C. Andreasen. A New Method for the In Vivo Volumetric Measurement of the Human Hippocampus with High Neuroanatomical Accuracy. *Hippocampus*, 10(6):752–758, 2000.

- [80] E. Parzen. On Estimation of Probability and Mode. *Annals of Mathematical Statistics*, 33:1065–1076, 1962.
- [81] A. Petterson, F. Walter, and D. Lagunovsky. Detection of Agricultural Fields in Satellite Images. In *Proceedings of NJF seminar, Remote Sensing in Agriculture*, pages 103–108, Jokioinen, Finland, 1996.
- [82] B. T. Phong. Illumination for Computer Generated Pictures. *Comm. of the ACM*, 18(6), June 1975.
- [83] R. Pierson, P. W. Corson, L. L. Sears, D. Alicata, V. Magnotta, D. S. O’Leary, and N. C. Andreasen. Structural MR Image Processing Using the BRAINS2 Toolbox. *NeuroImage*, 17:61–76, 2002.
- [84] J. P. W. Pluim, J. B. A. Maintz, and M. A. Viergever. Image Registration by Maximization of Combined Mutual Information and Gradient Information. *IEEE Transactions on Medical Imaging*, 19(8):809–814, 2000.
- [85] P. Ranefall, K. Wester, and E. Bengtsson. Automatic Quantification of Immunohistochemically Stained Cell Nuclei using Unsupervised Image Analysis. *Analytical Cellular Pathology*, 16(1):29–43, 1998.
- [86] R. A. Robb and C. Barillot. Interactive Display and Analysis of 3-D Medical Images. *IEEE Transactions on Medical Imaging*, 8(3):217–226, September 1989.
- [87] M. Rosenblatt. Remarks on Some Nonparametric Estimates of a Density Function. *Annals of Mathematical Statistics*, pages 642–669, 1956.
- [88] H. G. Schnack, H. E. H. Pol, W. F. C. Baaré, W. G. Staal, M. A. Viergever, and R. S. Kahn. Automated Separation of Gray and White Matter from MR Images of the Human Brain. *NeuroImage*, 13(1):230–237, January 2001.
- [89] W. Schroeder, K. Martin, and B. Lorensen. *The Visualization Toolkit: An Object-Oriented Approach To 3D Graphics*. Prentice Hall, 1996.
- [90] G. Sedvall. Monoamines and Schizophrenia. *Acta Psychiatrica Scandinavica, Supplementum*, 358:7–13, 1990.
- [91] J. Serra. *Image Analysis and Mathematical Morphology*, volume 1. Academic Press, 1982.
- [92] J. Serra, editor. *Image Analysis and Mathematical Morphology Volume 2: Theoretical Advances*, volume 2. Academic Press, 1988.

- [93] M. K. Österlund, C. Halldin, and Y. L. Hurd. Effects of Chronic 17β -estradiol Treatment on the Serotonin 5-HT_{1A} Receptor mRNA and Binding Levels in the Rat Brain. *Synapse*, 35(1):39–44, 2000.
- [94] R. Stokking, K. L. Vincken, and M. A. Viergever. Automatic Morphology-Based Brain Segmentation (MBRASE) from MRI-T1 Data. *NeuroImage*, 12(6):726–738, December 2000.
- [95] R. Stokking, K. Zuiderveld, H. Pol, P. Rijk, and M. Viergever. Normal Fusion for Three-Dimensional Integrated Visualization of SPECT and Magnetic Resonance Brain Images. *Journal of Nuclear Medicine*, 38:624–629, 1997.
- [96] C. Studholme, D. L. G. Hill, and D. Hawkes. Automated 3D Registration of MR and PET Brain Images by Multiresolution Optimisation of Voxel Similarity Measures. *Medical Physics*, 24(1):25–35, 1997.
- [97] C. Studholme, D. L. G. Hill, and D. Hawkes. An Overlap Invariant Entropy Measure of 3D Medical Image Alignment. *Pattern Recognition*, 32:71–86, 1999.
- [98] H. Suzuki and J. Toriwaki. Automatic Segmentation of Head MRI Images by Knowledge Guided Thresholding. *Computerized Medical Imaging, Graphics*, 15(4):233–240, July–August 1991.
- [99] R. Szeliski and S. Lavalle. Matching 3-D Anatomical Surfaces with Non-rigid Deformations Using Octree-splines. In *IEEE Workshop on Biomedical Image Analysis*, Seattle, June 1994.
- [100] J. Talairach and P. Tournoux. *Co-planar Stereotactic Atlas of the Human Brain: 3-dimensional Proportional System—an Approach to Cerebral Imaging*. Thieme Verlag, Stuttgart/New York, 1988.
- [101] L. Thurfjell. *An Adjustable 3D Brain Atlas for Quantitative Analysis of Neuroimaging Data: Algorithmical and Methodological Aspects*. PhD thesis, Uppsala University, May 1994.
- [102] L. Thurfjell, C. Bohm, and E. Bengtsson. CBA - an Atlas Based Software Tool Used to Facilitate the Interpretation of Neuroimaging Data. *Computer Methods and Programs in Biomedicine*, 47(1):51–71, 1995.
- [103] L. Thurfjell, C. Bohm, T. Greitz, and L. Eriksson. Transformations and Algorithms in a Computerized Brain Atlas. *IEEE Transactions on Nuclear Science*, 40:1187–1191, 1993.

- [104] L. Thurfjell, G. Lindahl, and R. Lundqvist. Fusion of Multimodality Brain Images. In *Proceedings of 11th Scandinavian Conference on Image Analysis, Kangerlussuaq, Greenland*, pages 359–365, 1999.
- [105] K. Varnäs, H. Hall, P. Bonaventure, and G. Sedvall. Autoradiographic Mapping of 5-HT_{1B} and 5-HT_{1D} Receptors in the Post Mortem Human Brain Using [³H]GR 125743. *Brain Research*, 915(1):47–57, 2001.
- [106] K. Varnäs, C. Halldin, and H. Hall. Autoradiographic Distribution of Serotonin Transporters and Receptor Subtypes in the Human Brain.
- [107] K. Varnäs, C. Halldin, V. W. Pike, and H. Hall. Distribution of 5-HT₄ receptors in the postmortem human brain - an autoradiographic study using [¹²⁵I]SB 207710. *Eur Neuropsychopharmacol*, 13(4):228–234, 2003.
- [108] P. Viola and W. M. Wells III. Alignment by Maximization of Mutual Information. In *Proc. 5th Int. Conf. Computer Vision*, pages 16–23, 1995.
- [109] F. Wehrmann, E. Bengtsson, and L. Thurfjell. A 3D Deformable Surface Model to Segment the Brain in MR Images. In *Proceedings of 11th Scandinavian Conference on Image Analysis, Kangerlussuaq, Greenland*, volume I, pages 289–294, 1999.
- [110] W. Wells, P. Viola, H. Atsumi, S. Nakajima, and R. Kikinis. Multi-Modal Volume Registration by Maximization of Mutual Information. *Medical Image Analysis*, 1:35–52, 1996.
- [111] C. Wählby, J. Lindblad, M. Vondrus, E. Bengtsson, and L. Björkesten. Algorithms for Cytoplasm Segmentation of Fluorescence Labelled Cells. *Analytical Cellular Pathology*, 24(2,3):101–111, 2002.
- [112] R. Woods, J. Mazziotta, and S. Cherry. Automated Image Registration. In U. Uemura, N. Lassen, T. Jones, and I. Kanno, editors, *Quantification of Brain Function, Tracer Kinetics and Image Analysis in Brain PET*, pages 535–547. Elsevier Science Publishers, Amsterdam, 1993.
- [113] R. P. Woods, S. T. Grafton, J. D. Watson, N. L. Sicotte, and J. C. Mazziotta. Improved Methods for Image Registration. *Journal of Computer Assisted Tomography*, 22:153–165, 1998.
- [114] A. P. Zijdenbos, B. M. Dawant, R. a., and A. C. Palmer. Morphometric Analysis of White Matter Lesions in MR Images: Method and Validation. *IEEE Transactions on Medical Imaging*, 13(4):716–724, December 1994.

- [115] M. Özkan, B. M. Dawant, and R. J. Maciunas. Neural-Network-Based Segmentation of Multi-Modal Medical Images: A Comparative and Prospective Study. *IEEE Transactions on Medical Imaging*, 12(3):534–544, September 1993.
- [116] S. W. Zucker. Region Growing: Childhood and Adolescence. *Computer Graphics and Image Processing*, 5:382–399, 1976.

Explanations of acronyms, abbreviations, and terms

Acronyms and abbreviations

2D Two dimensional

3D Three dimensional

AC-PC Anterior commissure to the posterior commissure

ANN Artificial neural networks

APG Activity projection grey level gradient shading

CBA Computerised brain atlas or when applicable Centrum för bildanalys
(Centre for Image Analysis)

CNS Central nervous system

CSF Cerebrospinal fluid

CT Computed tomography

CTA Computed tomography angiography

DSA Digital subtraction angiography

fMRI Functional magnetic resonance imaging

HUBIN Human brain informatics

IMP Image processing, the image analysis program used and developed at
CBA

IR Inversion recovery

KDE Kernel density estimates (continuous histogram)

MIP Maximum intensity projection

MR Magnetic resonance

MRA Magnetic resonance angiography

MRI Magnetic resonance imaging

NMR Nuclear magnetic resonance

PD Proton density

PET Positron emission tomography

RF Radio frequency

ROI Region of interest

T1 Longitudinal relaxation time

T2 Transversal relaxation time

SPECT Single photon emission tomography

VOI Volume of interest

Terms

6-connectivity A voxel is 6-connected if only its neighbours that share a face are considered as connected.

AC-PC-line A line from one structure in the brain, the anterior commissure, to another part of the brain, the posterior commissure.

Binary An image that consists of only two levels, i.e., black and white, is a binary image.

Computed Tomography A method to reconstruct slices of an object from X-ray beams. An attenuation map that is reconstructed.

Dilate Growing a region; binary objects become larger and grey-level images become brighter.

Erode Eroding a region; binary objects become smaller and grey-level images darker.

Functional magnetic resonance imaging Using MRI but a different time sequence to produce images with functional information.

Image processing Takes an image as input, processes it and creates an output image.

Image analysis Takes an image as input, extracts information and returns numbers.

Imaging The process of capturing data

Magnetic resonance imaging A method to reconstruct slices of an object using quantum effects when a magnetic field changes direction frequently

Morphology A mathematical way to describe how an image can be altered when applying a structuring element.

Neuroimaging Methods that take images of the brain.

Positron emission tomography A method to reconstruct slices of an object showing the physiological parameters. A radioactive substance is injected into the patient. Two gamma-photons emitted when a positron is annihilated in a collision with an electron are detected simultaneously.

Pixel Picture element, i.e., the smallest element of a digital image. The size of the pixel does not necessarily correspond to actual spatial resolution.

Ray-casting A method to construct a 2D image from a 3D volume.

Rendering The process of generating 2D images from a 3D data set.

Resolution The smallest extent of an object detectable in an image.

Segmentation To choose region(s) from an image.

Shading effects In MRI there are variations in the grey-levels throughout the volume. These variations are due to inhomogeneities of the magnetic field created by the coils in the scanner.

Single photon emission tomography A method to reconstruct slices of an object showing the physiological parameters. A method similar to PET but with lower resolution. It shows the concentration of radio-nucleids admitted to the patient.

Surface rendering A visualisation technique that uses a geometric model of the objects displayed. The model is described with geometric primitives such as points, lines, triangles or arbitrary polygons and uses standard computer graphic techniques to render the data.

T1-weighted A time sequence for MRI (longitudinal relaxation time). Fat appears as very bright. White matter is also bright and grey matter is somewhat darker. Fluids and bone are very dark. Air gives the lowest brightness.

T2-weighted A time sequence for MRI (transversal relaxation time). Fat appears as very bright. White matter is also bright and grey matter is somewhat darker. Fluids are very bright and bone are very dark. Air gives the lowest brightness.

Tomography A method to reconstruct slices of an object.

Vertex A corner point in a geometric model.

Volume rendering A visualisation method that operates directly on 3D data and takes into account the changing properties inside the volume.

Voxel Volume picture element, i.e., the smallest element of a digital image volume. The size of the voxel does not necessary correspond to actual spatial resolution.

Tesla The System International (SI) unit of magnetic flux density, equal to one Weber per square meter. Symbolised T.

Colour Plates

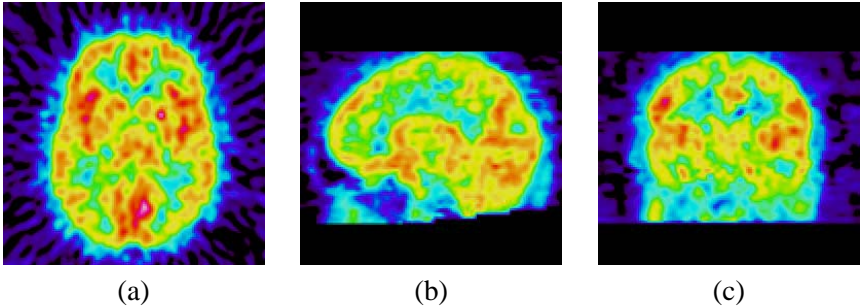


Figure 1.3: An activation from a PET image of the brain, showing transaxial, sagittal, and coronal slices.

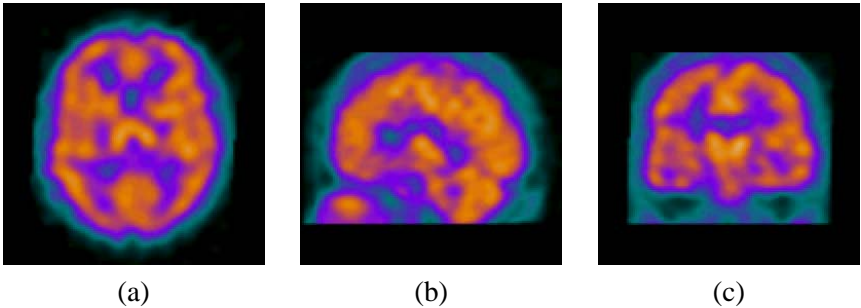


Figure 1.4: An activation from a SPECT image of the brain, showing transaxial, sagittal, and coronal slices.

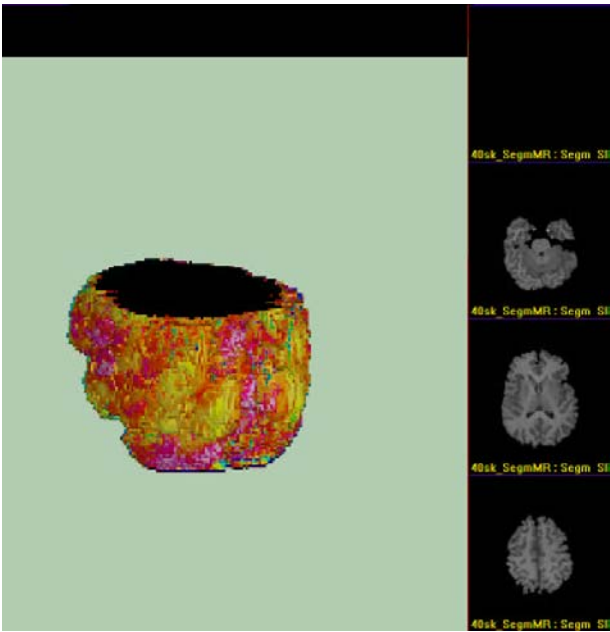


Figure 1.5: A 3D visualisation in CBA 5.0.

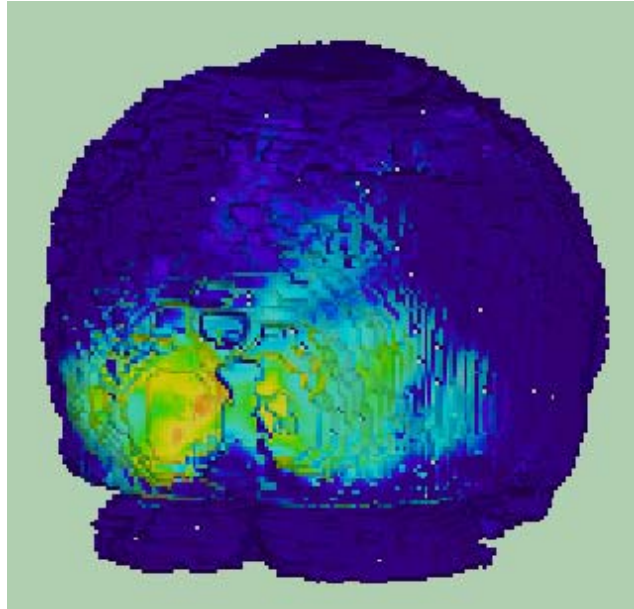


Figure 3.3: Activated regions of a fMRI mapped onto a segmented MRI which has been visualised using volume rendering.

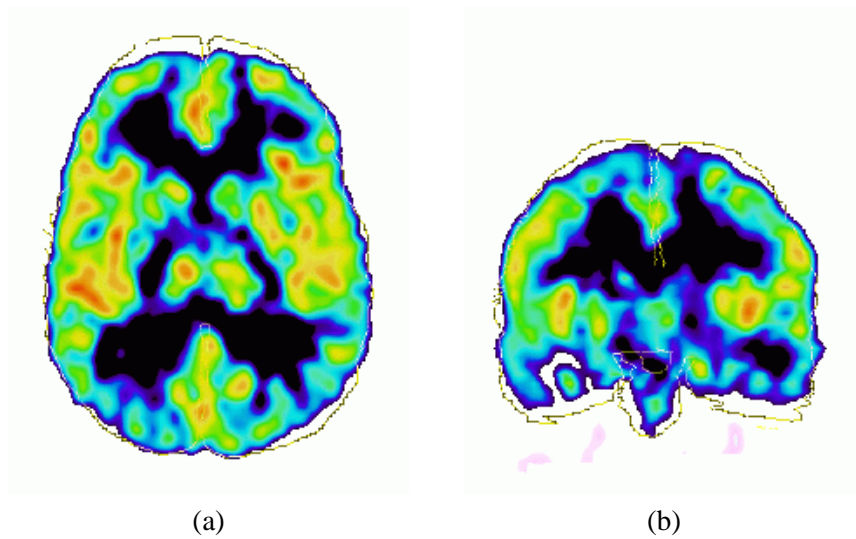


Figure 3.4: An activation of the brain. A transaxial slice (left) and a coronal slice (right) with the contours of the brain atlas that are used as an anatomical reference.

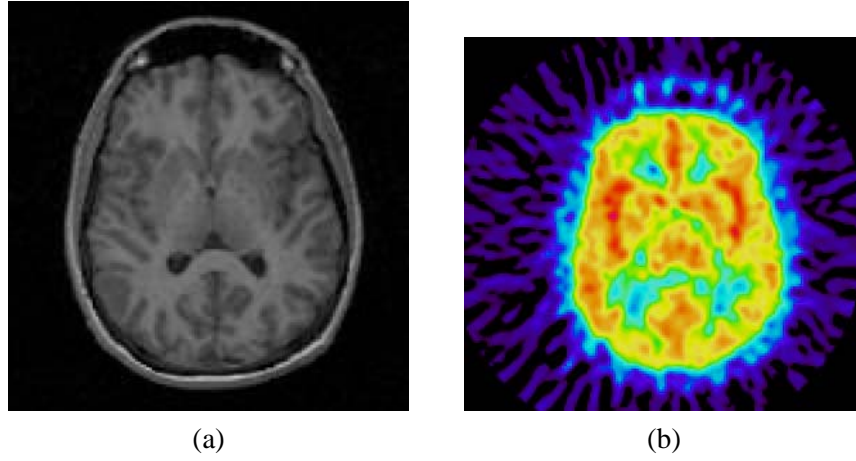


Figure 3.5: The original a) MRI and b) PET volumes.

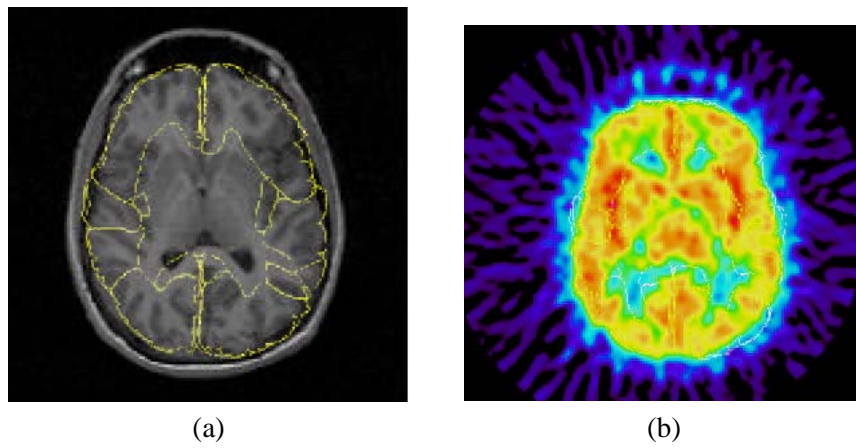


Figure 3.6: The a) MRI and b) PET volumes with structures from the computerised brain atlas.

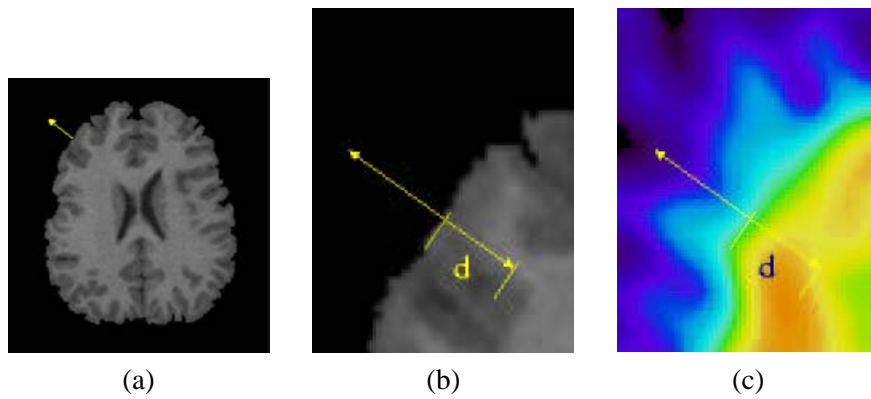


Figure 3.7: a) Segmented MRI with b) normal and c) PET with the same normal and depth to be checked.

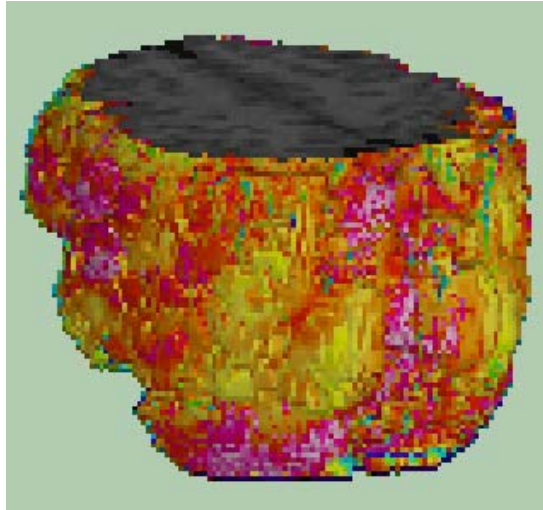


Figure 3.8: The same data as in Figure 3.4. The APG method was used to map the activated areas onto the surface of segmented MRI of the same patient.

